Fluvial-lacustrine interactions in the Marginal Triassic, Clevedon, Bristol Channel Basin, UK: deposition, dolomitization and silicification

Corresponding author:
Maurice Tucker;
Email: maurice.tucker@bristol.ac.uk

Maurice E. Tucker and R. Stephen J. Sparks

School of Earth Sciences, University of Bristol, Bristol, UK

Abstract

In the Triassic Mercia Mudstone Group of the Bristol Channel area, SW Britain, yellow micritic-oolitic dolomites deposited in a near-shore location of an extensive shallow saline alkaline lake, pass landwards into conglomerates and sandstones of colluvial-fluvial origin (Dolomitic Conglomerate). Offshore facies are red marl (Branscombe Fm.) and grey-green marl (Blue Anchor Fm.) of shallow lake-playa origin. Conspicuous red silicified bands and nodules (cherts) occur within the shoreline dolomites cropping out at Clevedon, 30 km SW of Bristol. The originally aragonitic ooids and lime mud were dolomitized very early on the lake floor and just below, and the presence of pyrite indicates anoxic conditions therein. The silicification is attributed to the influx of meteoric water with near-neutral pH, provided by flash floods and rainstorms as hyperpycnal and hypopycnal flows, interacting with the silica-rich, saline, alkaline lake water and porewater within the lake sediment. Aragonitic ooids picked up in the flows underwent dissolution, then slight compaction of outer dolomitic lamellae, before silica precipitation. The red colour of the chert from detrital finely disseminated hematite also indicates very early precipitation, before suboxic-anoxic conditions developed in the enclosing lake carbonates. These Triassic sediments show features of soft-sediment deformation, attributed to the formation of chert via a silica gel and/or density contrasts of rapid deposition-dewatering, plus possible seismic activity connected to a nearby basin-margin fault.

1. Introduction

There are numerous examples in the stratigraphic record of fluvial deposits interfingering with lacustrine sediments. Well-documented examples occur in the Eocene Green River Fm. of Utah (Gall *et al.* 2017; Birgenheier *et al.* 2020), the Eocene-Miocene of the Madrid Basin (Bustillo *et al.* 2002; Reijmer *et al.* 2020), the Triassic Ordos Basin, China (Zavala *et al.* 2020) and the Devonian Orcadian Basin in NE Scotland (Andrews & Hartley, 2015). Modern-Quaternary examples have been described from desert basins in the western U.S.A. (e.g. Bristol Dry Lake and others, Lowenstein & Risacher, 2009), Africa (e.g. Chad Basin, Shettima *et al.* 2018) and Australia (Lake Eyre Basin, Mann & Amos, 2022). However, there are few detailed accounts of the consequences of the interactions between meteoric water, which may deliver clastic sediment through a pluvial-fluvial system to a lacustrine environment, and the lake water and porewater within the lacustrine sediments. The input of fluvial sediment to a lake, as a result of a flash flood for example, commonly results in erosional features (scours and channels), depositional structures (cross-bedding, ripples, etc.) but also soft-sediment deformation (disturbed-disrupted bedding, sand/mud dykes and volcanoes). A further effect is the mixing of waters with different chemistries, for example, near-neutral pH, fresh-meteoric water (rainstorms and floods), also cold, mixing with alkaline more-saline lake waters, and warm, if under an arid climate. Such mixing may cause mineral precipitation, notably of silica, giving chert beds and nodules, and carbonate, as well as alteration-dissolution of other minerals, particularly during syn-sedimentary and early shallow-burial diagenesis.

Chert beds and nodules are common features in carbonate rocks throughout the stratigraphic record but there has always been a debate over the origin of the silica and how it was precipitated (Tucker, 2023a). In marine facies, a biogenic source is commonly invoked, notably diatoms, radiolarians and sponge spicules composed of opaline silica, along with volcanic influences. In continental settings, both abiotic and biotic processes may be involved in SiO_2 precipitation, taking place in three main situations: hot springs (sinters), in some cases associated with volcanic activity and hydrothermal fluids, as in East Africa (Renaut *et al.* 2002), alkaline lakes (e.g. the Coorong, S. Australia, Peterson & von der Borch, 1965) and within soils (silcretes, pedogenic and groundwater), relatively common in South Africa and Australia (e.g. Ullyott & Nash, 2016; Taylor & Eggleton, 2017).

This paper documents intercalated fluvial and lacustrine carbonate-clastic facies, from the Upper Triassic Mercia Mudstone Group (MMG) of the Bristol Channel Basin, notably in the
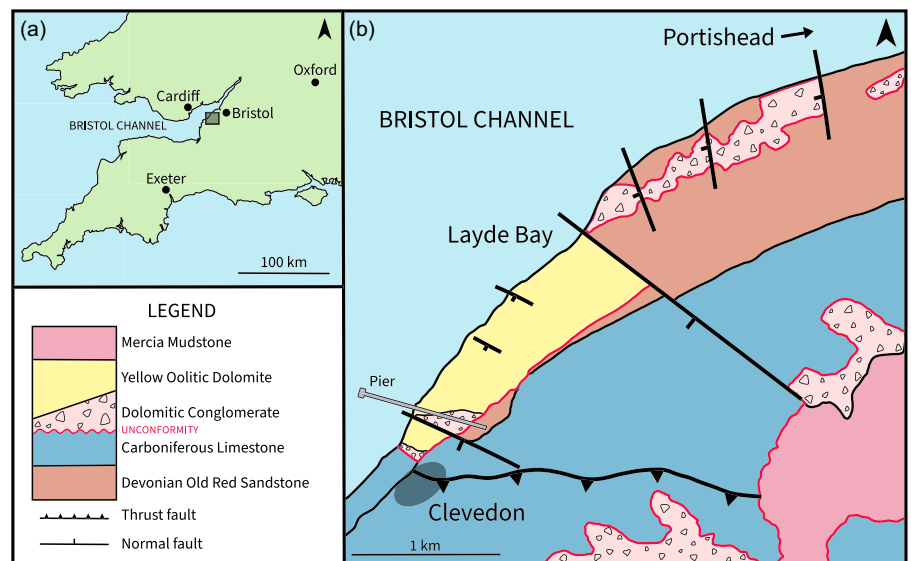
Figure 1. (a) Location map of the Clevedon-Portishead area in NW Somerset. (b) Local geology around Clevedon: Triassic Mercia Mudstone strata resting on Palaeozoic rocks. After Milroy (1998).
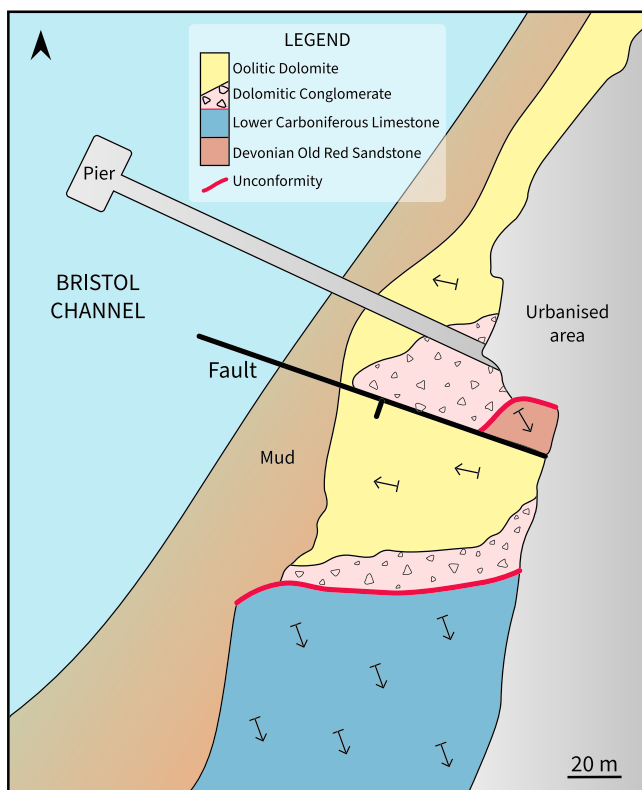

Figure 2. Detailed geological map of the area around Clevedon Pier, NW Somerset.

vicinity of Clevedon and Portishead, NW Somerset, SW England (Figures 1 and 2). These lacustrine dolomitic sediments include conspicuous red silicified layers and nodules (cherts) along with some enigmatic features and distinctive diagenetic patterns. We investigate the sedimentology and diagenesis of these marginal lake facies and from field, petrographic and geochemical data show that the silicification was related to pluvial/fluvial-lacustrine water interactions, rather than being of pedogenic – groundwater (silcrete) origin. The climate was arid to semi-arid (Milroy & Wright, 2000; Milroy et al. 2019) and there were likely influences from syn-sedimentary extensional fault activity as well as later

hydrothermal fluids and mineralization. Triassic sediments similar to those of the MMG in SW Britain were also deposited extensively across the North Sea into western Europe, notably France and Germany (e.g. Vollemer et al. 2008), as well as in the Newark Basin of eastern North America (Smoot, 1991) and in the SW USA (e.g. the Chinle Fm., Tanner, 2000), plus East Greenland (Clemmensen et al. 1998). This period was characterized by widespread and long-lived aridity, high global temperatures and extensive desert conditions across the supercontinent Pangea, shortly before its disruption, but with occasional pluvial-fluvial interludes, as in the Carnian for example (e.g. Baranyi et al. 2019).

2. Geological setting

The Upper Triassic (Carnian, Norian and lower Rhaetian) MMG (237-206 Ma) of southwest Britain is dominated by a thick (100s of m) succession of monotonous red dolomitic mudstone deposited in extensive inland basins, with at times likely connections to the distant open ocean to the south-southwest. These depocentres, which include the Wessex, Somerset, Bristol Channel, Worcester and Cheshire basins, on the western side of England, were mostly extensional basins associated with the very early stages of the opening of the North Atlantic (Chadwick & Evans, 1995; McKie & Williams, 2009; Husein et al. 2022). The upper red part of the MMG (the Branscombe Fm.) is succeeded by the Blue Anchor Fm. (formerly the Grey and Tea Green Marls), which extends from the uppermost Norian into the early Rhaetian (Figure 3) (Warrington, 1974; Warrington et al. 1980; Howard et al. 2008). The succeeding Penarth Group (206–201 Ma) consists of variable mostly fine-grained facies and contains numerous fossils of brackish to lagoonal origin. These transitional facies gradually became more marine, eventually giving way to the fully marine, moderate depth, fine-grained limestones and mudstones of the Blue Lias of the Lower Jurassic.

In the Bristol-Glamorgan areas particularly, the red and grey-green MMG marls gradually onlap the Palaeozoic basement, mostly Pembroke Limestone Gp. (Carboniferous Limestone)-Coal Measures Gp. and Devonian Old Red Sandstone (ORS) strata. In these areas, **basin-margin facies** are developed with lacustrine-playa, littoral-sublittoral, fluvial and colluvial-pedogenic facies (Tucker, 1978; Milroy & Wright, 2000; Howson et al. 2022). In the
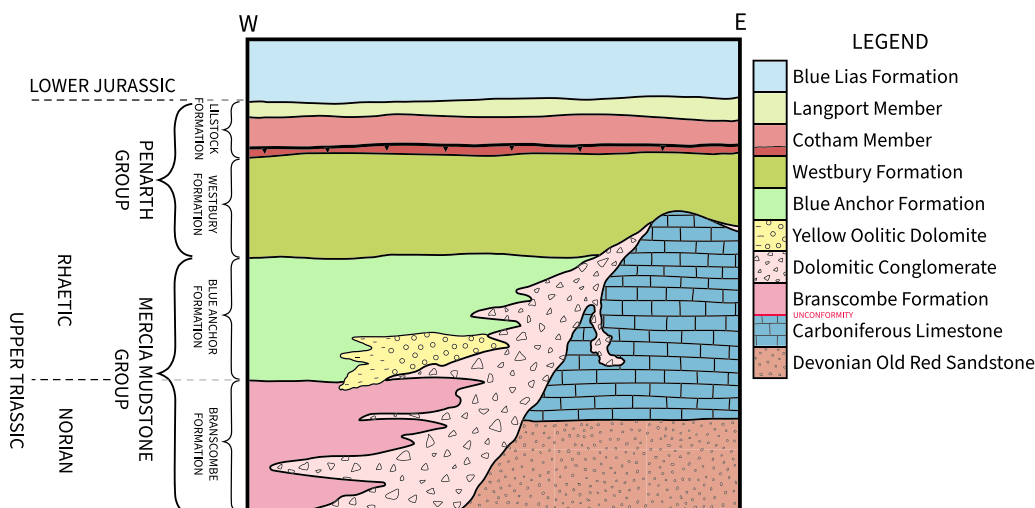
Figure 3. Schematic cross-section of the Bristol Channel Basin margin in the late Triassic–early Jurassic, with strata onlapping an Upper Palaeozoic topography. The yellow oolitic dolomites are the subject of this paper.

Bristol-Mendips area, these rocks have been informally referred to as the **Dolomitic Conglomerate (DC),** although genuine conglomerates are only one of several lithofacies. These facies in the Bristol Channel area have been described by Tucker (1977, 1978), Waters & Lawrence (1987), North (1988), Leslie *et al.* (1992, 1993, 1995), Milroy & Wright (2000, 2002), Porter & Gallois (2008) and Howson *et al.* (2022).

Clevedon Beach adjacent to Clevedon Pier in North Somerset exposes littoral and lacustrine facies of the uppermost MMG with prominent red bands of silicification (cherts) within dolomitized limestones. The geology along Clevedon Beach is very varied and complex in a relatively small area (Figure 2). There are outcrops of fluvial Devonian sandstone, marine Lower Carboniferous strata with a variety of body and trace fossils, and the Upper Triassic sediments of this study, ranging from fluvial to lacustrine breccias, conglomerates, sandstones and oolitic carbonates, with relics of evaporites (gypsum). The Devonian and Carboniferous strata are folded, being located on the southern limb of a large-scale regional anticline. Minor parasitic folds and thrust-faults are observed along the beach outcrops. Rocks adjacent to and within a major fault at the Pier (Figure 2) are conspicuously mineralized with pink baryte and galena occurring in veins and as matrix to fault-related breccias. Part of the location has been designated a Site of Special Scientific Interest (Grid Ref ST 4015-7185, Natural England SMB-304, 1992) in view of its Lead-Copper-Zinc-Arsenic-Baryte mineralization related to this major fault (Ixer *et al.* 1993). At least 30 hypogene and supergene minerals have been identified. To the north of the Clevedon Bay fault, that is between Clevedon Pier and Ladye Bay, 1 km north, the Triassic sediments consist of dolomitized oolites overlying DC, resting on ORS (Figure 1) (Milroy & Wright, 2000, 2002). There is then another fault on the N side of Ladye Bay where the Triassic lacustrine oolites are up against ORS.

3. Methods

From routine fieldwork in the Clevedon-Portishead area, samples were collected, cut and polished, and petrographic observations were made on thin-sections with Leica and Nikon photomicroscopes. Geochemical analyses were undertaken at the University of Leicester, School of Geography, Geology and the Environment. Major elements were determined on a Rigaku ZSX Primus IV WD-XRF (Wave Dispersive – X-Ray Fluorescence) spectrometer using fused glass beads prepared from ignited powders with a sample-to-flux ratio of 1:7.5 and a 66% Li tetraborate: 34% Li metaborate flux. The results are quoted as component oxide weight percentages, re-calculated to include LOI (loss on ignition). Trace elements were analysed on a PANalytical Axios Advanced WD-XRF spectrometer using 32 mm-diameter, pressed-powder pellets produced from mixing 7 g finely-ground sample powder with 12–15 drops of a 7% PVA solution, and (Moviol 8-88) pressed at 10 tonnes per sq. inch. Rare earths were determined using a Thermo iCAPQ ICP-MS (inductively-coupled plasma-mass spectrometer). SEM (scanning electron microscope) observations and EDS (energy dispersive spectrometer) analyses were undertaken in the School of Earth Sciences, University of Bristol, using a Hitachi S-3500N with a Thermo-Fisher EDS system.

Although no new isotope analyses were undertaken for this project, published whole-rock isotope data of similar facies in the Bristol Channel region are included to support interpretations here. These analyses, Leslie *et al.* (1992, 1993) and Milroy (1998), using standard techniques with results expressed in ‰ Pee Dee Belemnite (PDB), were undertaken at the British Geological Survey isotope geochemistry facility.

4. The Triassic at Clevedon-Portishead

The Triassic basin-margin facies exposed on the beach at Clevedon (Figure 4) crop out along much of the coast to Portishead, 5 km NE (see Ashley *et al.* 2024 for a field-guide to this coast). The major fault running ESE-WNW across the beach about 5 m to the south of Clevedon Pier (Figures 1, 2, and 4) creates a 10 m high cliff, composed of immature Triassic polymictic breccias (DC). These pass up and laterally seawards into yellow micritic-oolitic carbonates, appearing dark from coastal weathering (Figure 4 a). These sediments rest unconformably in the NE corner of the beach on Devonian Portishead Fm., consisting of fractured, large-scale cross-bedded grey litharenite. The bedded Triassic rocks dip gently to the west, although it is not clear if this dip represents original draping of palaeo-topography or has a tectonic origin. Immediately to the south of the fault, almost horizontally bedded (dip 2–3° W) cream to yellow littoral Triassic lacustrine dolomites with interbedded red silicified bands and nodules (cherts) and lenses of blue-green marl, the focus of this paper, crop out across a 100 m wide, gravel-boulder strewn foreshore (Figures 4 a, 5 a). Several minor faults on the foreshore splay off the major fault, disrupting the lacustrine dolomites and blue-green marl. Farther to

Figure 4. (a) Cliff at Clevedon Pier, view west, defined by major E-W fault (blue dashed line), with Devonian Old Red Sandstone (ORS) unconformably overlain by Triassic Dolomitic Conglomerate (DC) which passes up into yellow Triassic oolitic dolomite (YD). On the foreshore, south of the main fault, there are several minor splay faults, and the yellow dolomite is partly covered by gravel and boulders. (b) Blue-grey marl between 2 minor splay faults on foreshore with adjacent yellow dolomite.
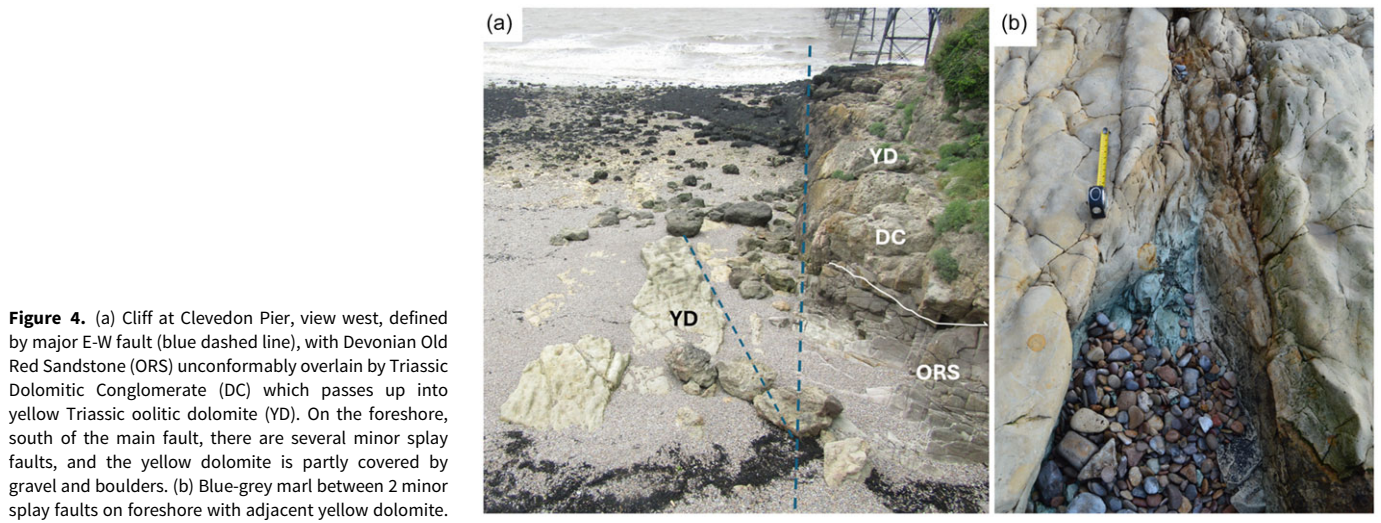

Figure 5. (a–e) Foreshore south of Clevedon Pier, covered in pebbles, showing yellow oolitic dolomite with layers and nodules of silicified red sediment (black arrows in Fig. 5 a), weathering proud, showing undulations and disturbed features of the red chert bands.

the south (100 m), the Triassic dolomites pass laterally along the beach to the southwest into a coarse basal breccia of Palaeozoic clasts resting unconformably on the marine, fossiliferous Shirehampton Fm. of the lowest Carboniferous, which dips to the southeast (Figure 2).

5. Sedimentary facies of the Marginal Triassic sediments at Clevedon

Two major Mercia Mudstone Group facies associations are distinguished here in NW Somerset: A) Lacustrine facies and B) Fluvial-colluvial siliciclastic facies (features summarized in Table 1).

5.a. Lacustrine facies

At Clevedon, these consist of three interbedded sub-facies: 1) dominant *yellow dolomites* with common ooids and some siliciclastic grains, and various sedimentary structures, 2) beds, bands and nodules of *Red silicified rock* (chert) and 3) limited outcrops of *Blue-grey marl*. In addition, 4) in many parts of NW Somerset, there are *Red marls* ('Keuper' facies) but these are not exposed in the Clevedon area and are best seen at the classic Aust Cliff exposure (25 km NE) and along the North Somerset coast (e.g. St Audrie's Bay to Blue Anchor). The yellow dolomites with the red cherts represent the sublittoral to littoral facies marginal to the extensive lake-inland sea to the south-southwest (wherein the red and blue-grey marls were deposited), and close to a hilly-rocky shoreline immediately to the east and northeast of Upper Palaeozoic strata, supplying siliciclastic material by fluvial-colluvial processes.

5.b. Fluvial-colluvial siliciclastic facies

The Dolomitic Conglomerate in the greater Bristol-Mendips area includes 1) *Breccias*, massive to thick-bedded, varying from clast to matrix supported with a red muddy-sandy dolomitic matrix, clasts composed of Devonian and Carboniferous sandstone and lime-stone-dolomite, along with clasts of Triassic soil/regolith, referred to as pedorelicts (Howson *et al.* 2022). These are colluvial-scree and local debris-flow deposits. 2) *Bedded breccio-conglomerates* and *coarse sandstones*: medium to thick-bedded sandy conglomerates, pebbly coarse sandstones to finer sandstones, commonly channelled with erosive bases and local cross-bedding. These are mostly stream flood deposits. 3) Well-bedded sandstones-silt-stones-mudrocks, with cross-bedding, lamination and ripples, being sandy to muddy channel to floodplain deposits and 4) locally interbedded *pedogenic facies* (nodular calcretes) and *hiatal surfaces* (horizons of exfoliated-cracked pebbles on upper surfaces of breccia/conglomerate), representing extended periods of soil development and subaerial exposure. These various facies are well displayed further NE along the coast towards Charlcombe Bay, 3.5 km NE of Clevedon. See Milroy (1998) and Howson *et al.* (2022) for further information.

5.c. Field observations

Yellow dolomites are mostly poorly bedded with vague lamination and bedding on the mm to cm scale. In places, they display medium-scale cross-bedding (sets 20 cm high) (Figure 6 a) and flat bedding with relics of wave-formed ripples. Most beds consist of clay-grade (lime mud-dolomicrite) to sand (oolitic-peloidal) grade carbonate (Figure 6 b), with minor quartz and lithic sand grains.

There are local concentrations of granules to small pebbles of basement clasts (ORS and Carboniferous Limestone), together with cm-size clasts of blue-grey and red marl (Figure 7 a). There are also thin micritic beds of mm-scale, irregular-crinkly lamination of likely microbial-mat-biofilm origin and some cm-thick micritic layers broken up into intraclasts (Figure 7 b). In places, the bedding is disturbed, manifested by flat marl clasts defining a foliation, which can be vertical. Up to 2 m of section are exposed on the Clevedon foreshore, but in the cliff below the Toll-House, on the north side of the fault, up to 8 m of yellow dolomite crop out above 2–3 m of breccia facies, becoming more oolitic upwards and seawards, with less siliciclastic material, similar to the succession at Ladye Bay, 1 km NE.

Within the yellow dolomites exposed in the mid to high part of the foreshore at Clevedon, there are conspicuous bands and nodules of extremely hard **red silicified rock**, which range from near-continuous flat to undulating 'pavement' surfaces through to discontinuous layers in the form of discrete lenses and nodules (Figures 5 a–e, 8 a, b). The cherty bands typically range in thickness from 5 to 10 cm and form a resistant cap to foreshore exposures of the much softer, more porous yellow dolomite (Figures 5 a–e). In some places, the red silicified bands are beds with coarser clastic sediment than the adjacent yellow dolomites (Figure 8 a), along with scattered small basement pebbles up to 3 cm in diameter. Elsewhere, the red bands are similar to adjacent carbonates in terms of clastic content or grain size, simply appearing as diagenetic nodules of red chert within the dolomite (Figure 8 b). There are cm-scale patches of yellow dolomite within the silicified red bands (Figure 8 a, b).

The bases of the red bands vary from fairly regular, near-horizontal and parallel to bedding in adjacent yellow dolomite to undulating with an apparent erosive base, to be more irregular, disrupted and deformed with downward penetrating lobes and protrusions (Figures 5 b–d, 8 a, b). In some places, there is a thin (mm), finer-grained basal layer to the silicified bands. The upper surfaces of the chert layers are smooth to undulating with hollows and ridges; locally, they appear to be distorted, with fold-like structures and local 'gaps' in the bands (Figures 5 b–d). These features suggest that at some earlier time, the bands were soft and ductile, unlike their present hard, brittle nature. Displacements of one band by up to 15 cm indicate local soft-sediment faulting.

In one place in a silicified red bed, there is an intriguing feature of two divergent elongate lobes about 8 cm long (Figure 9). The feature resembles structures with three lobes in similar-aged Marginal Triassic sediments in South Wales, interpreted as dinosaur footprints (Tucker & Burchette, 1977). Overall, the observations of deformation, faulting and loading indicate that at a time either during or soon after its formation these layers were soft, ductile and malleable.

Discrete silicified nodules are present in the yellow dolomites, notably near the low tide mark of the beach at Clevedon, several metres below the horizons of the red silicified bands. The nodules, white/cream to pink-red in colour, are a few cm up to 10 cm across, round to oval to elongate in shape (Figures 10 a, b). In cut section, however, the outer surface of the nodules is cauliform (Figure 10 b). The nodules mostly consist of fine-grained quartz, but coarser, clear, colourless, glassy crystals are present in their centre, or they are hollow, like geodes. Similar nodules are present in Ladye Bay (Milroy & Wright, 2000).

Blue-grey marl crops out over a square metre or more below the beach gravel about mid-tide, 5 m south of Clevedon Pier, 50 m west of the seawall. This outcrop appears to be within the yellow

Table 1. Features of the lacustrine and fluvial facies of the Mercia Mudstone Group

Lacustrine Facies	Mineralogy	Grain size	Sedimentary structures	Interpretation
1: Yellow dolomite	Dolomite, some clay, calcite, quartz, rare feldspar, pyrite, goethite	Micrite to sand (ooids), some coarse	Lamination, beds, flat-cross-beds, microbial laminites	Low to moderate energy, nearshore marginal lake
2: Red silicified beds, bands, nodules	Silica-quartz, some dolomite-calcite, rare feldspar, Fe^{3+} oxides.	Fine to coarse sand, few small pebbles	Some grading, soft-sediment deformation	Fluvial-flood water input to lake, early chert precipitation
3: Grey-green marl	Mostly clay + Fe^{2+}, quartz silt, dolomite-calcite	Fine <20 microns	Massive to laminated, local brecciation	Shallow lake, low energy to playa, suboxic, humid
4: Red marl	Mostly clay, quartz silt, Fe^{3+} oxide, dolomite-calcite, local gypsum	Fine <20 microns	Massive to laminated, palaeosoil horizons	Shallow lake, low energy to playa, subaerial, oxic, arid
Fluvial facies	**Mineralogy**	**Grain size**	**Sedimentary structures**	**Interpretation**
1. Coarse breccia	Mixed, varied clasts, Palaeozoic limestone, sandstone, pedorelicts	Sand to boulder grade	Massive, weak bedding, no/poor sorting, clast and matrix support	Scree /colluvium, terrestrial, arid
2: Conglomerate to sandstone	Mixed, varied clasts, Palaeozoic limestone, sandstone	Silt to pebble grade	Sorted conglomerates, massive to well-bedded, cross-beds, channels	Debris-stream flows, flash floods, arid
3: Sandstone, siltstone	Quartz, minor feldspar, calcite	Clay to sand grade	Well-bedded, cross-beds, lamination, ripples, desiccation cracks	Stream-sheet floods, ponded water, arid
4: Pedogenic facies, hiatal exposure surfaces	Quartz, carbonate, clay	Fine to coarse sand, pebbles	Nodules, mottles, rootlets, exfoliated pebbles, sheeted bedrock	Pedogenic, soil, weathered bedrock surfaces, arid

Figure 6. (a) Cross-bedded oolite, set height 20 cm, on south-facing cliff beneath Clevedon Pier. Field of view 1 m across. (b) Photomicrograph of oolitic dolomite. Field of view 2 mm across. Thin-section courtesy of Eric Squires.
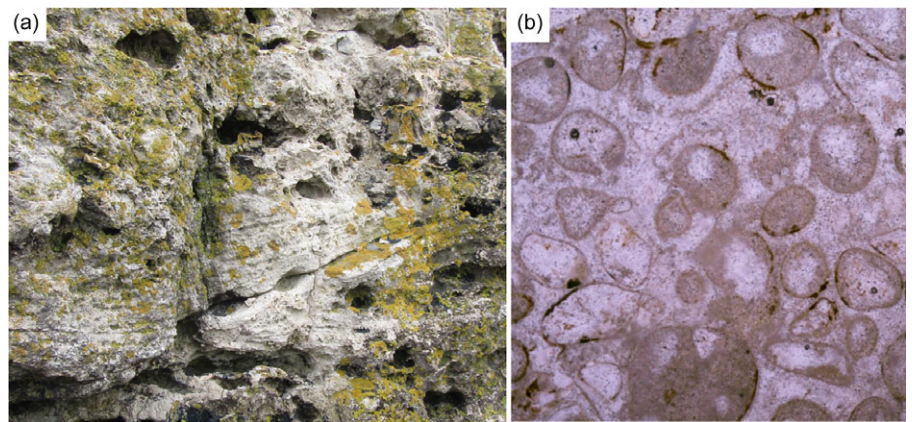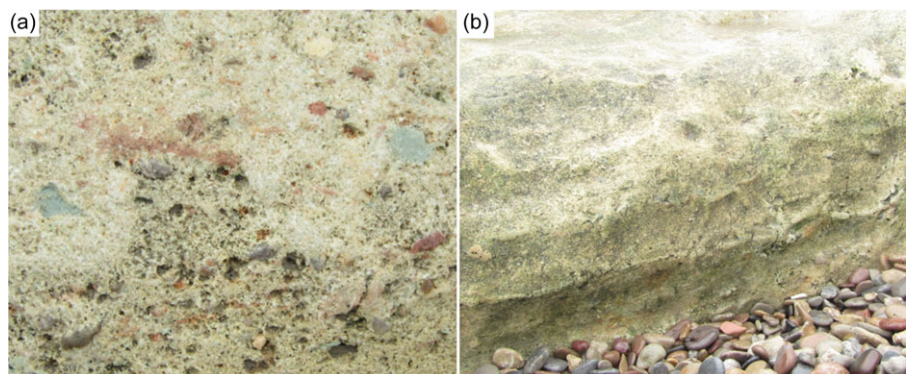

Figure 7. (a) Yellow oolitic dolomite with scattered small pebbles and clasts of red and green marl-siltstone. Field of view 20 cm across. (b) Yellow oolitic dolomite with thin beds of dolomicrite disrupted into clasts. Field of view 40 cm across.
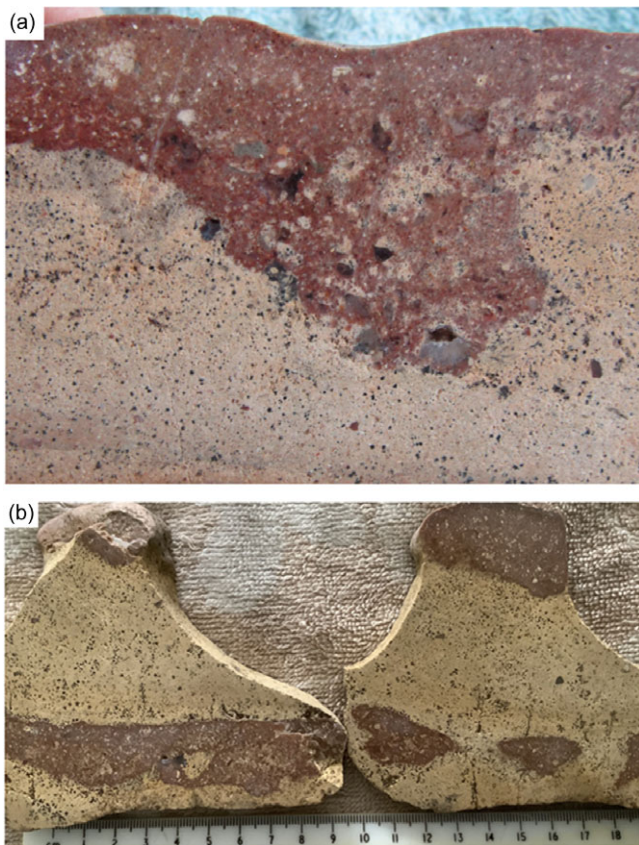
Figure 8. (a) and (b) Cut surfaces of chert bands within yellow dolomite. In (a) coarser sediment within the silicified band, an irregular base to the chert layer from erosion or loading into less dense dolomitic sediment. Cm-scale areas of yellow sediment within the chert. In (b) two cut surfaces of a large block with 2 chert bands: the lower is continuous to nodular, and the upper is seen (in the field) to be a more continuous band. The dark spots and streaks in the yellow dolomite are late diagenetic Mn-oxides and dendrites. All slabs are ~ 10 cm across.
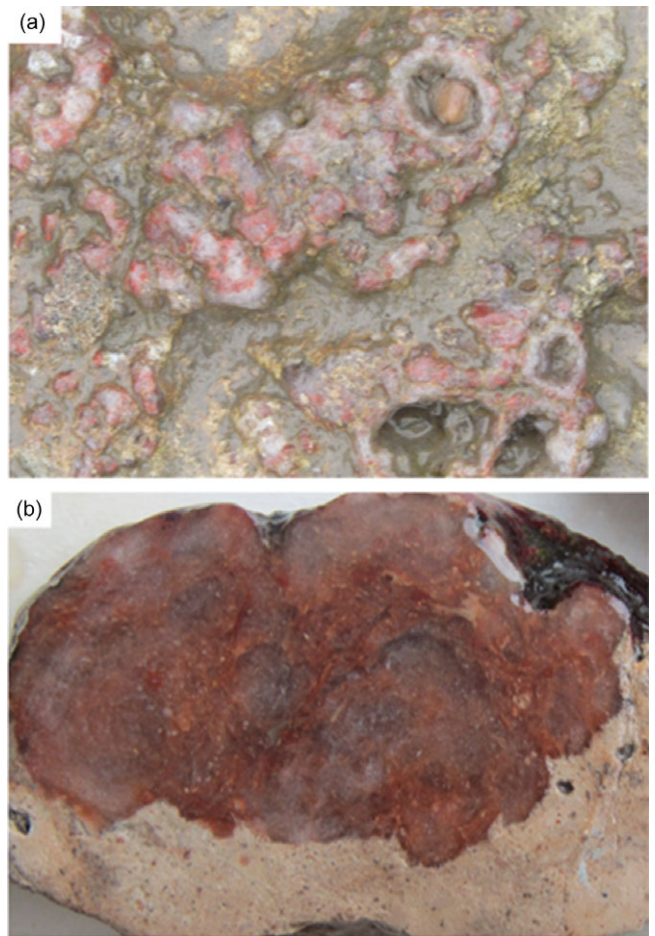

Figure 10. (a) Quartz nodules, white to red in colour, some with central voids containing quartz crystals, within micritic-oolitic dolomite. Field of view 15 cm across. (b) Cut surface showing red quartz nodule with botryoidal outer margin. Field of view 10 cm across.

Figure 9. Red silicified sediment layer with a possible dinosaur footprint (20 cm long) on the upper surface showing 2 toes.

oolitic dolomites. Marl also occurs between the major fault and a minor splay fault 30 m from the seawall (Figure 4 b). In a temporary excavation in 2000, at least 80 cm thickness of blue-grey marl was observed behind the seawall above yellow dolomites and adjacent to the major fault itself (Mathieson in Ashley *et al.* 2024). These blue-grey marls at Clevedon Pier are dolomitic mudstones varying in appearance from fissile to blocky, in some places breaking with a conchoidal fracture. Although in the field they appear homogeneous, massive and structureless, like typical mudstones, on cut surfaces, a remarkable range of features is revealed: mm-scale lamination with silty graded layers, wispy and vaguely folded lamination, and brecciated units with rounded to angular clasts (Figure 11 a, b).

6. Petrography of Marginal Triassic lacustrine facies

6.a. Yellow micritic-oolitic dolomites

This microfacies consists of both fine- and coarse-grained/ crystalline varieties. The finely crystalline carbonate micrite matrix contains local to abundant carbonate grains and scattered siliciclastic grains. Numerous small dolomite rhombs, 10–20 μm diameter, commonly vague to poorly defined in thin-section, occur throughout the fine matrix, but there are also scattered larger,
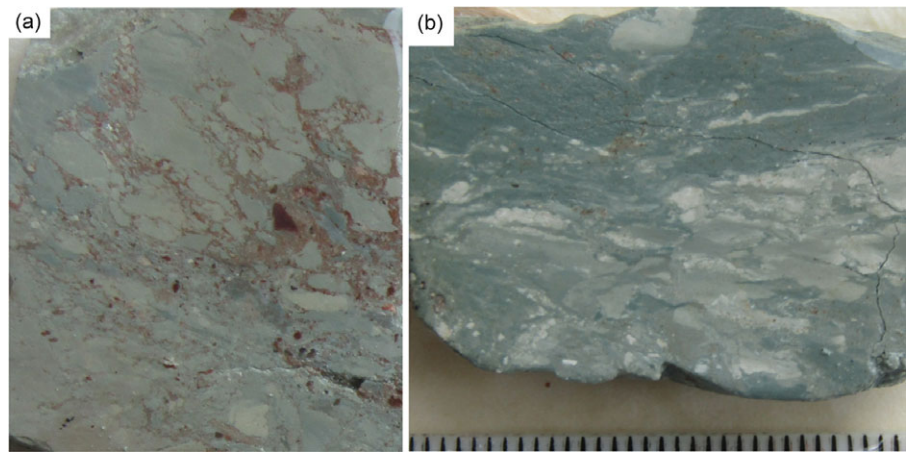
Figure 11. (a) and (b) Cut surfaces of grey-blue marl showing a range of features: Laminated, brecciated, angular to elongate clasts of different shades of grey, some red sediment. From exposure on Clevedon foreshore. Scale mm.
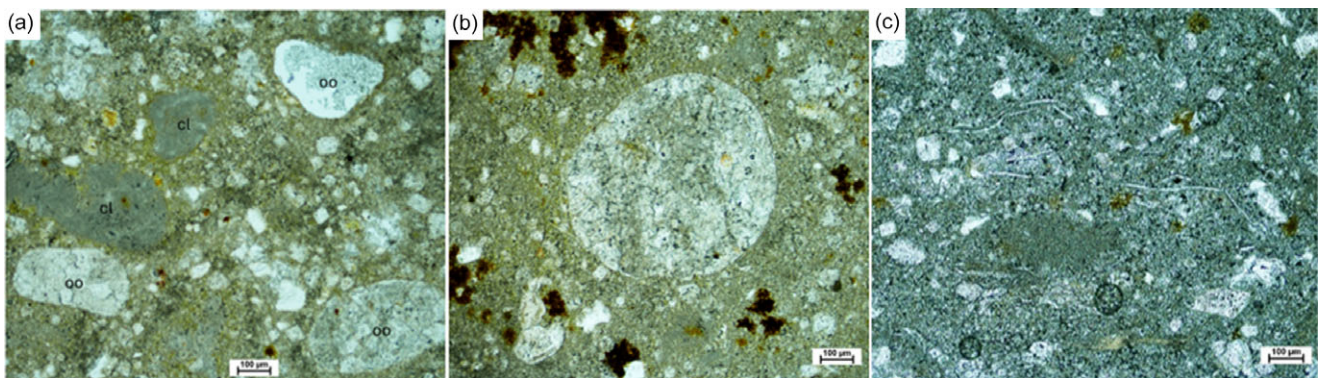

Figure 12. Yellow oolitic–micritic dolomite. (a) Three dolomitized ooids (oo), 2 grains of Carboniferous Limestone (grey, cl), quartz silt and scattered dolomite rhombs, in a fine dolomitic micrite. (b) Ooid with well-defined outer lamella in fine dolomite sediment with quartz silt and patches of oxidized pyrite (dark brown). (c) Fine-grained dolomite with vague sand-sized grains, scattered larger dolomite rhombs and fragments of carbonate rafts (thin sheets). Scale bars each 100 microns.

better-formed dolomite rhombs up to 100 μm across (Figures 12 a–c). In many places, the dolomicrite has a vague peloidal appearance (grains 250–500 μm diameter), composed of tiny (5 μm) carbonate particles. Sand-sized carbonate grains are mostly 0.5–1 mm in diameter and many consist of micritic carbonate, such that they could be peloids. These are interpreted as micritic grains of faecal or microbial origin (synsedimentary); some could be reworked and altered fragments of Carboniferous Limestone which formed the upland areas adjacent to the lake margin. The ooids themselves are round through to ovoid-subrounded in shape, mostly in the range of 300–700 μm diameter (Figures 6 b, 12 a, b). They mostly consist of dolomite crystals within an obvious outer lamella, 5–10 μm thick composed of very fine micritic dolomite. With some ooids, the outer lamella is a red coating, a few μm thick, not always continuous (Figure 6 b). The dolomite crystals within the ooids are fine to coarse, subhedral (planar-s) to non-planar in shape, varying from limpid to cloudy and poorly defined (Figures 6 b, 12 a, b). In some cases, empty spheroidal voids are inferred to be oomolds. Nuclei in the ooids are rare. These ooids show the same features as the dolomitized ooids described from Ladye Bay (Milroy & Wright, 2002).

The silicate grains are mostly of quartz with minor feldspar and are present in two size grades: silt (20–50 μm), disseminated throughout, and sand-size, 500 μm to 1.5 mm. Some beds would classify as a silty dolomite. Within the yellow carbonates are conspicuous 100–500 μm-sized areas of rusty brown iron oxide-hydroxide, likely goethite-limonite (Figures 13 a–c). They vary

from spheroidal to crystal shapes (cubic-triangular-hexagonal) and appear to consist of sub-particles. Under reflected light, areas of bright yellow-silver colour observed within the brown patches are relics of pyrite (Figure 13 b). Elsewhere there are dendrite-looking features of the same rusty brown colour.

In areas of the foreshore close to the major fault, the yellow dolomites have numerous fractures with a spacing of 5–10 cm containing galena in patches up to a cm across. Greenish copper carbonate minerals (malachite) are rare and white to pink baryte is a common fracture fill. Pyrolusite (MnO_2) occurs as scattered mm-sized black spots in the dolomite (as in Figure 8 b) and as dendrites, branching out from the fractures. Liesegang rings are present on dolomite surfaces (Ashley, 2014).

Silt to fine sand-sized feldspar crystals of K-feldspar and albite were observed in the SEM (see Figures 17 a, 18 a) and could be authigenic, although rarely reported in limestone (e.g. Singewald & Milton, 1929; Hearn & Sutter, 1985). Tiny (<5 μm) baryte crystals are evenly distributed through the sediment and minor rutile is noted (Figure 17 a).

6.b. Red silicified bands and nodules (cherts)

This microfacies mostly consists of a red-brown fine-grained matrix of microquartz with vague micritic sand-sized grains (peloids) (Figures 14 a, b), along with other grains. There are scattered well-developed dolomite rhombs, 20–50 μm in size. Some of these larger dolomite rhombs have irregular margins when in
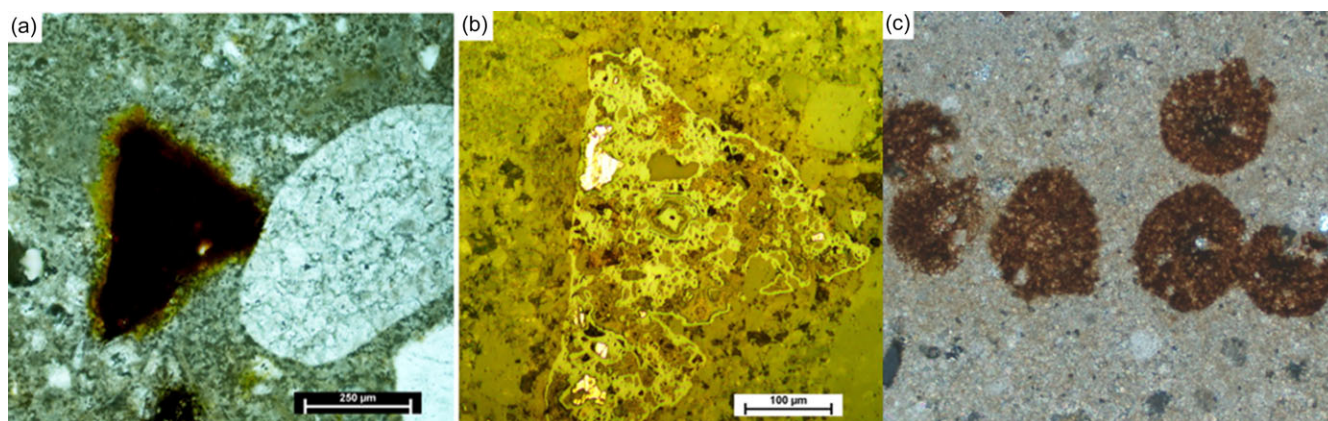
Figure 13. (a) Oxidized pyrite and dolomitized ooid in yellow micritic dolomite with quartz silt. Scale bar 250 microns. (b) Reflected light view of (a) pyrite relics in oxidized material. Scale bar 100 microns. (c) Oxidized pyrite spheres and crystal forms, 200 microns diameter, in dolomitic micrite with some larger scattered dolomite rhombs.
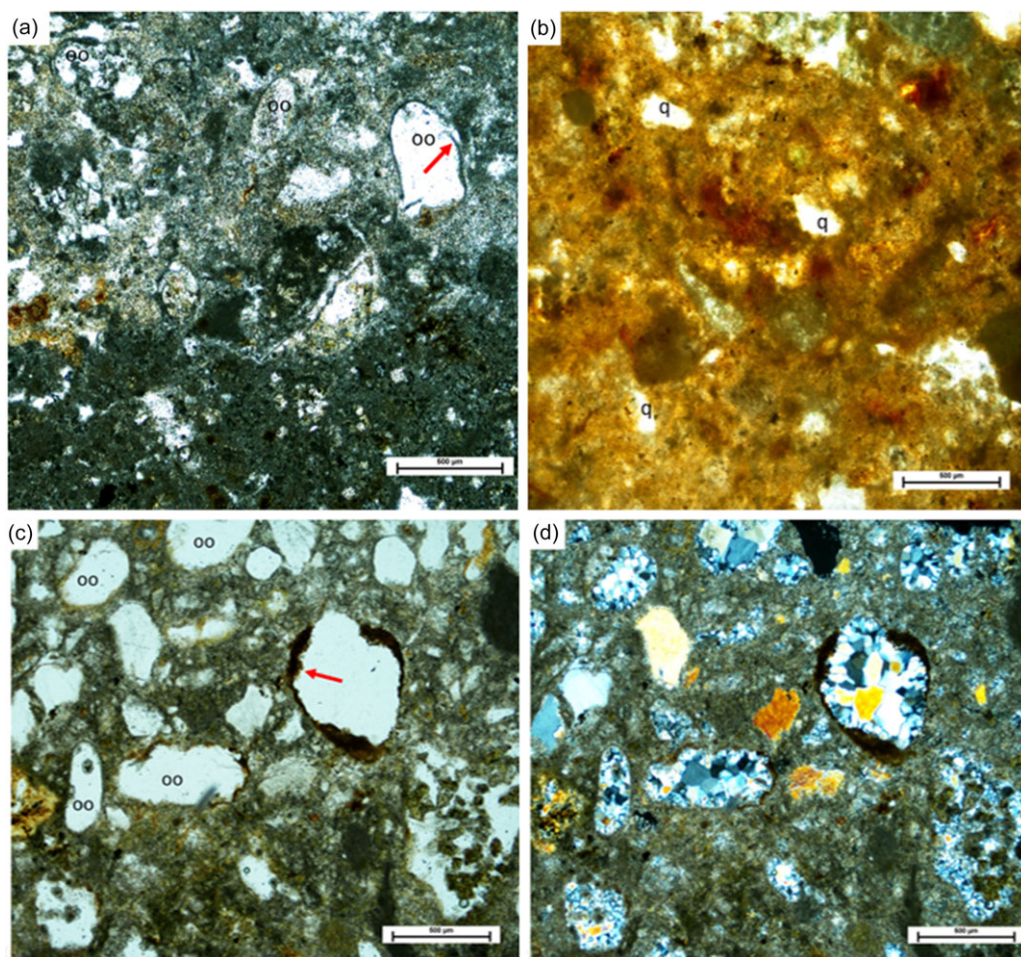

Figure 14. (a) In upper part, red sediment with silicified ooids (oo, one with fractured outer lamella, red arrow) and other grains, fine silica matrix and scattered silt-sized quartz grains, and below, dark fine-grained (yellow) micritic dolomite, vaguely peloidal. (b) Red silicified sediment with vague relics of sand-sized grains and scattered quartz silt (q). (c) and (d) Red silicified sediment with grains of quartz, some of which silicified ooids (oo); one grain with partial clay coat (red arrow), plane polarised light (PPL) and crossed polars (XP). All scale bars are 500 microns.

contact with the silica (Figure 17 b), indicating reaction with the fluid precipitating the silica. Around 10% of the rock consists of detrital quartz grains, minor feldspar and lithic grains, fragments of siltstone, mudrock and Carboniferous Limestone, including individual fossils, especially crinoid debris. Many grains are medium sand but larger grains are present, up to 10 mm across. Some grains are partially to fully coated with a thin dark red-brown rim (Figure 14 c, d).

Round sand-size grains composed of quartz crystals commonly show a drusy fabric (i.e. increasing crystal size towards the grain centre), with a thin, dark outer rim (5 μm thick) of very fine dolomite (Figures 15 a–d, 17 c, 18 b). In some cases, this outer rim has fractured and been displaced, like a broken eggshell (Figures 15 a–d), and the quartz crystals include the fractured lamella and extend outside the former grain into the original intergrain pore space. The drusy texture of this quartz indicates it is a cement filling a void, attributed to dissolution of an aragonitic ooid. The minor fracture and breakage of the outer lamellae before the quartz precipitation indicate very early quartz precipitation just
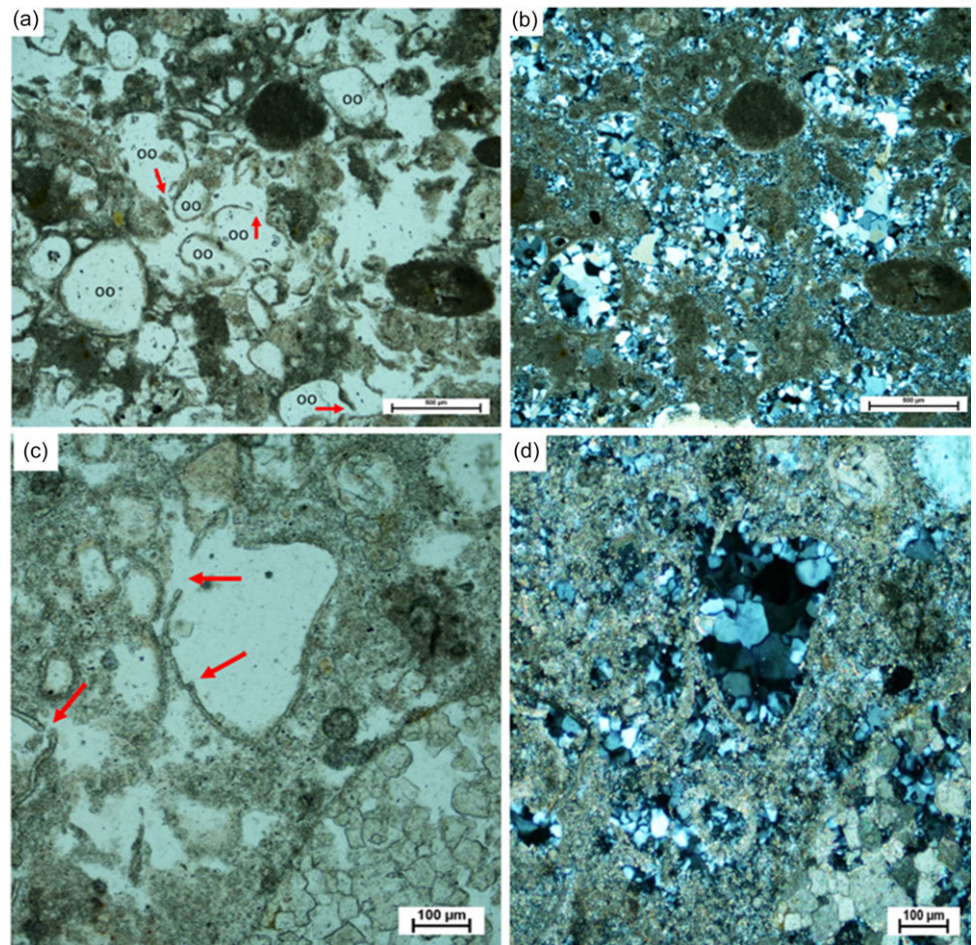
Figure 15. Red silicified sediment with ooids (oo) showing clear outer lamella, in some cases fractured (red arrows), and fill of drusy quartz, which extends into adjacent original pore space, in a matrix of silicified lime/ dolomitic mud. (a) and (b): scale bars 500 microns, PPL and XP. (c) and (d): scale bars 100 microns, PPL and XP.
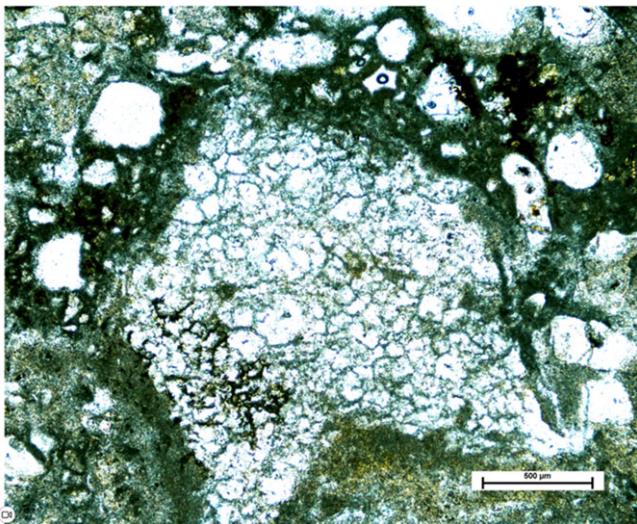

Figure 16. Former gypsum crystal with a red micritic coating, now consisting of quartz in a lacey-alveolar texture (microbial/pedogenic), within red silicified sediment containing silicified ooids. PPL, scale bar 1000 microns.

after aragonite dissolution, as compaction was beginning but before any significant burial.

The red colour of this silicified sediment is attributed to finely disseminated iron oxide (hematite). There are no relics of pyrite present. One case of a gypsum pseudomorph is inferred from a

swallow-tail crystal shape (500 μm across) with a fine-grained red-brown clay-micrite rim (Figure 16) and a quartz interior. Some detrital grains contain dolomite rhombs, clear to cloudy, which are floating in a medium crystalline quartz matrix. These dolomite rhombs were clearly present before the silicification; they could be reworked fragments of Carboniferous dolomite, with some early dissolution then silica cement.

7. Geochemistry and mineralogy

7.a. Sediment geochemistry

We present major and trace element analyses of two samples of each rock type (Table 2). The two analyses of each sample type are extremely close in element contents. The most obvious and unsurprising difference between the compositions is the much higher silica content of the chert.

The main mineral assemblage of the **yellow carbonate** is dolomite, calcite and detrital quartz with minor feldspar and Fe oxide (see Figures 17, 18). This mineral assemblage is consistent with the major element chemistry. Dolomite and smaller amounts of calcite account for the inventory of MgO, CaO and LOI (assumed to be almost entirely CO_2). SiO_2, Al_2O_3, Na_2O and K_2O can be explained by detrital quartz and alkali feldspars. Fe_2O_3 is explained by the iron oxide-hydroxides. There is minimal S, indicating low contents of sulphide (relic pyrite) or sulphate (baryte). We can use mass balance on the average of the two compositions to calculate approximate wt% proportions of

Table 2. Chemical data for Yellow dolomite and Red chert; oxides in % and group 1 and 2 trace elements in ppm

Oxides	Yellow Dolomite 1	Yellow Dolomite 2	Red Chert 1	Red Chert 2	Ratio Dolomite/Chert
SiO_2	17.93	18.77	62.95	66.93	
TiO_2	0.11	0.12	0.05	0.05	2.10
Al_2O_3	1.90	1.88	0.90	0.92	2.06
Fe_2O_3	1.40	1.34	0.66	0.68	2.04
MnO	0.36	0.37	0.15	0.13	2.61
MgO	15.87	15.31	7.42	6.67	2.21
CaO	25.15	25.70	11.36	9.99	2.38
Na_2O	0.11	0.15	0.05	0.05	2.60
K_2O	0.70	0.60	0.32	0.32	2.03
P_2O_5	0.07	0.07	0.04	0.03	2.00
SO_3	0.12	0.09	nd	nd	
LOI	36.79	36.42	17.06	14.99	2.05
Total	100.51	100.76	100.95	100.77	
Group 1					
Ga	2.8	2.2	1.4	1.5	1.72
La	8.0	10.0	4.4	4.1	2.17
Nd	9.6	14.7	6.5	6.2	1.92
Rb	19.4	18.6	10.3	9.8	1.89
Zr	56.9	51.7	29.8	28.6	1.86
V	20.1	20.1	9.5	9.1	2.16
Y	15.6	15.4	7.7	7.3	2.05
Group 2					
As	25.5	46.7	6.8	4.4	6.45
Mo	2.4	3.9	1.0	0.9	3.31
Ba	2153.4	1458.5	386.4	159.0	6.60
Co	15.5	29.4	1.40	3.0	10.20
Cu	87.7	158.0	21.40	38.5	4.10
Pb	7.9	6.9	2.4	1.8	3.52
Zn	289.7	698.7	101.9	57.6	6.19
Sr	147.3	200.2	48.0	37.1	4.08
Nb	3.9	3.8	2.6	2.8	1.43
Ni	26.0	76.9	6.8	32.6	
Th	2.3	1.7	1.0	<0.4	
U	1.0	1.2	2.7	2.8	0.40

dolomite (72%) and calcite (10.5%). The Al_2O_3, Na_2O and K_2O contents are consistent with a few percent of detrital feldspar and small amounts of clay.

The **silicified red rocks** have substantial silica (chert) (~65%), as to be expected, and 32% dolomite. In Table 2 we list the ratio of each major element oxide in the yellow dolomite relative to that in the silicified red rocks. A key observation is that the ratio for most oxides is approximately 2 and this suggests that the system is largely closed except for the ingress of silica. Thus, the main geochemical differences between the rock types can simply be explained by the addition of silica.

Data on trace elements can be divided into two groups in terms of the ratios of each element in the two rock types. In one group (Ga, La, Nd, Rb, Zr, V, Y), the ratio is close to a value of 2. These are a diverse set of elements that in many geochemical systems might behave differently through interaction with fluids or physical separation of different mineral components due to sedimentary processes. However, whatever fluids were involved in the silicification process, they have not perturbed the geochemistry significantly for these elements beyond dilution as a consequence of the ingress of silica. There is also no significant difference in the ratio of dolomite to detrital silicate grains in the two rock types in
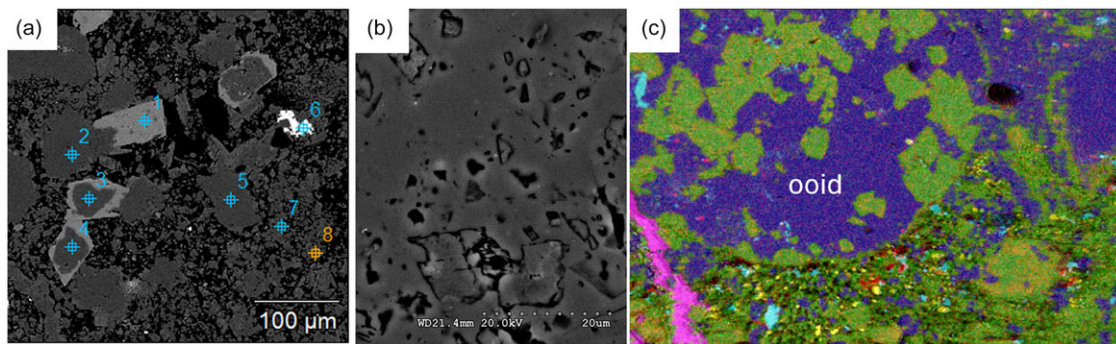
Figure 17. (a) Scanning electron microscope-back-scattered electrons (BSE) image of yellow dolomite sediment (point analyses 7, 8; Mg, Ca, O, C), with authigenic feldspar (point 1; Si, O, Al, K), quartz (points 2, 5; Si, O), albite (points 3, 4; Si, O, Al, Na) and rutile (point 6; Ti, Si, O). (b) SEM-BSE image of silica enclosing corroded dolomite rhombs, 10-15 microns in diameter. (c) SEM-EDS map of silicified-dolomitized ooid with calcite vein cutting through. Colours: green = Mg (dolomite), blue = Si (quartz), cyan = Al (K-spar), yellow = Ba (baryte), pink = Ca (calcite), red = Fe (iron oxide).
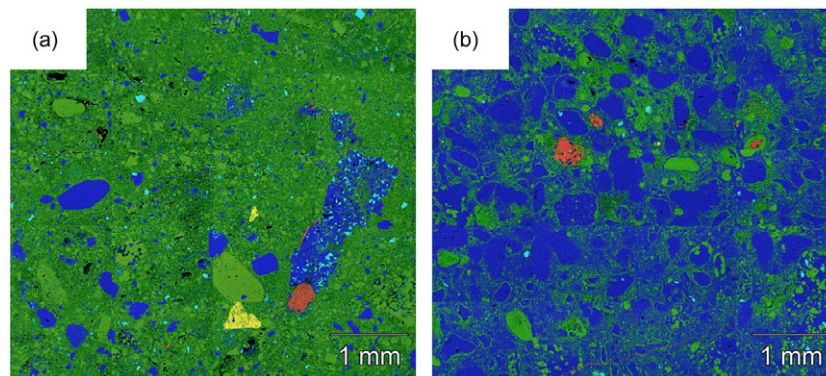

Figure 18. X-ray maps showing distribution of major elements for an area of (a) yellow dolomite sediment and B) red silicified sediment. Colours: green = Mg (dolomite), red = Ca (calcite), blue = Si (silica), cyan = Al (K-spar), yellow = Fe (pyrite-goethite). In (b), note the very thin dolomite outer lamella around the silicified ooids. Porosity measurements under SEM: dolomite sediment 25-35%; silicified sediment 5-6%, over an area roughly 10 mm × 10 mm.

the 2 samples analyzed. The second group of elements (As, Mo, Ba, Co, Cu, Pb, Zn, Sr) shows ratios much greater than 2 and these are likely to be those associated with the Pb–Cu–Zn mineralization. In the yellow dolomite, these elements can also be linked to the higher content of S and As as these elements are found in sulphide and sulphate mineral species (Ixer *et al.* 1993). The mineralization took place well after the silicification, so the simplest explanation of group 2 elements is that they are associated with infiltration of mineralizing fluids into the porous and permeable yellow dolomite, but these same fluids were prevented from ingress into the low porosity and permeability red silicified bands. There is one notable exception in that U is enriched in the silicified red bands compared to the yellow dolomite. U solubility in aqueous fluids is very sensitive to pH (Smedley & Kinniburgh, 2023), reaching a minimum at about pH = 8.5, and is also somewhat sensitive to Eh and activities of carbonate-bearing and other ionic species (Goodwin, 1982; Chudasama et al. 2018; Stanley & Wilkin, 2019). Thus, the U behaviour could be explained by changing fluid composition during silicification. The observation is consistent with a decrease in pH from around 9 to 7.5 through meteoric water input and mixing with lake water (discussed below).

A final issue is the extent to which the red cherts are formed by silica filling pore space or replacement of a fine carbonate matrix by silica. Of particular significance are the ratios of CaO and MgO since these relate to one of the major mineral constituents, dolomite. We observe that the ratio is 2.21, which is slightly greater

than the ratio observed in other major elements and group 1 trace elements. If we assume the silica only fills pores, then using mass balance, we find that adding silica to the yellow dolomite composition requires about 55% porosity. This interpretation can explain the typical ratio in major elements, including MgO, and Group 1 trace elements as a closed system dilution effect. If we then consider that the yellow dolomite contained 10% calcite and assume it was replaced by silica, the initial porosity would then reduce to 45%. The current porosity of the yellow dolomite is 25–35% and it has undergone burial compaction, so it seems plausible that the initial surface sediment in the lake had a porosity of 45%. Modern carbonate sediments do have porosities of these high values (oolitic sands are 45%, lime muds up to 70%; Enos & Sawatsky, 1981). If this was the case, then there is no requirement to replace the dolomite, assuming that dolomitization preceded silicification.

7.b. Stable isotopes

Although we present no new isotope data, it is instructive to discuss published analyses to inform interpretation of the depositional environment and diagenesis of the sediments. Leslie *et al.* (1993) presented whole-rock data from the Tea Green Marl (and the red Mercia mudstones below) from Somerset and South Devon and Milroy (1998) analysed samples from the Ladye Bay Oolite Member, all dolomites, equivalent to the yellow dolomites of

Table 3. Carbon-oxygen isotope data (‰ PDB) for Ladye Bay oolites (Milroy 1998), Tea Green Marl (Blue Anchor Fm.) from Somerset (Leslie *et al.* 1992) and calcrete-tufa-travertine from the Marginal Triassic, Glamorgan (Leslie *et al.* 1993)

	Oxygen	Carbon
Ladye Bay Oolites	1.5	−0.13
	1.55	0
	1.26	0.02
	1.3	0.34
	1.62	0.46
	2.2	0.36
Tea Green Marl	1.5	1.4
	0.7	0.9
	0.5	1.9
	1.2	2.2
	1.1	1.5
	1.6	1.1
Calcretes Glamorgan	−3.9	−2.6
	−4.1	−4.3
	−4.5	−5.2
	−4.7	−6.3
Tufa/travertine Glamorgan	−5.6	−2.3
	−4.9	−2.4
	−2.9	−3
	−5.2	−2.1
	−5.9	−3.8
	−5.6	−2.4

Clevedon (Table 3, Figure 19). The values from the Ladye Bay oolites are all very similar, with an average $\delta^{13}C$ PDB of 0.3 ‰ PDB (range −0.13 to +0.46 ‰ PDB) and $\delta^{18}O$ PDB of 1.5 ‰ PDB (range +1.3 to +2.2 ‰ PDB). For the Tea Green Marl, the $\delta^{13}C$ PDB values have a small heavier average of 1.5 ‰ PDB although there is a little more scatter (range +0.9 to +2.2 ‰ PDB); the $\delta^{18}O$ PDB values average 1.2 ‰ PDB (range 0.5 to 1.6 ‰ PDB), very similar to the oolites.

Leslie *et al.* (1992) presented data on calcretes and travertine-tufa from the Marginal Triassic of Glamorgan, and all $\delta^{13}C$ PDB and $\delta^{18}O$ PDB data therein are quite different from the oolites and marls at Clevedon, with low to very negative $\delta^{13}C$ PDB and moderately low to quite negative $\delta^{18}O$ PDB (average calcrete $\delta^{13}C$ PDB −4.4 ‰ PDB, $\delta^{18}O$ PDB −4.8 ‰ PDB; average travertine-tufa $\delta^{13}C$ PDB −2.7 ‰ PDB, $\delta^{18}O$ PDB −5.1 ‰ PDB).

8. Interpretations and discussion

8.a. Depositional environments and processes

The yellow dolomites possess many features consistent with deposition in a low to moderate energy location in the vicinity of a lacustrine – inland-sea shoreline. Cross-bedding and flat bedding indicate moderate wave-current activity, water depths in the region of 0.5–3 m, as in the equivalent facies exposed in Ladye Bay, 1 km to the north of Clevedon (Milroy & Wright, 2000). Ooids are typical of such locations and are forming today in the Great Salt Lake and Pyramid Lake, USA (Eardley, 1938; Popp & Wilkinson, 1983). The development of oolites in the Marginal Triassic is only documented from this eastern side of the Bristol Channel Basin, probably related to the shoreline orientation relative to prevailing winds. Periods of lower energy are indicated by finer-grained carbonates; these are likely to have been aragonitic-high magnesium calcite (HMC) lime muds. Crudely developed irregular lamination in this facies could be relics of microbial mats, as to be expected in lower energy areas of a shallow saline lake; local mud intraclasts indicate erosion of lithified crusts or subaerial exposure and desiccation. Occasional influx of terrigenous sediment through flash floods is indicated by the presence of siliciclastic silt and sand, either disseminated or in lenses and thin beds. The presence of dolomite and the dolomitization of the ooids are discussed below in the diagenesis section, but it is likely that the fine-grained dolomite was forming on the lake floor or just below within the sediment. A schematic model for deposition in this Triassic lake is presented in Figure 20.

The red silicified chert bands in some cases are associated with more clastic-rich sediment than the enclosing carbonates, and with their coarser grains up to small pebble size, the influx of sediment as events is indicated. This is consistent with the generally sharp, erosive bases of these red chert beds and the presence of clasts of yellow carbonate within these red beds as well. The influx of coarser sand and pebbles into the lake system attests to the influx of run-off waters and these could well have been in the form of a *hyperpycnal flow*, whereby a dense sediment-laden flow enters a water body and flows along the lake floor (e.g. Yang *et al.* 2017 for a Triassic example from the Ordos Basin) (see Figure 20). An input of terrigenous clastic material mixing with lake carbonate is envisaged in this case, resulting from a flash flood-debris flow from the hinterland following a major storm. The presence of ooids in these red chert bands would be the result of the mixing of incoming terrigenous material with oolitic sand forming in the lake. Tucker (1978) and Tucker & Burchette (1977) interpreted laterally extensive 10 cm-thick siliciclastic beds in the similar-aged Marginal Triassic of Glamorgan as sheet-flood deposits formed from shallow debris-stream flows into a lake-playa system.

However, as noted, there are also patches of red chert in the form of nodules and discontinuous bands where the sediment itself appears to be of similar grain size and composition (ooids + clastic grains) to the surrounding yellow carbonate. In these cases, the red chert appears to cut across the bedding, suggesting that the contact is a diagenetic front, indicating post-depositional silicification. With these silicified nodules, it is suggested there were still influxes of freshwater, but in the form of *hypopycnal flows* (flows less dense than that of the water body) transporting suspended clay-dust particles, which gave rise to the red colour (Figure 20).

The pervasive red colour of the silicified bands and nodules is attributed to detrital iron-containing clay/dust in suspension within the incoming flow. A dry-arid desert environment favours the accumulation of ferric oxide within terrigenous sediment, and the presence of ORS in the adjacent landscape would also have contributed fine-grained hematite. The Fe-rich coats around some grains could reflect pedogenesis in the hinterland.

In arid-zone lakes, sand and coarser sediment are invariably deposited relatively close to shore with finer clay in suspension being carried much farther offshore in a hypopycnal flow. This phenomenon is clearly seen in images from news outlets from the recent huge flash flood in Derna, Libya (September 2023) and has
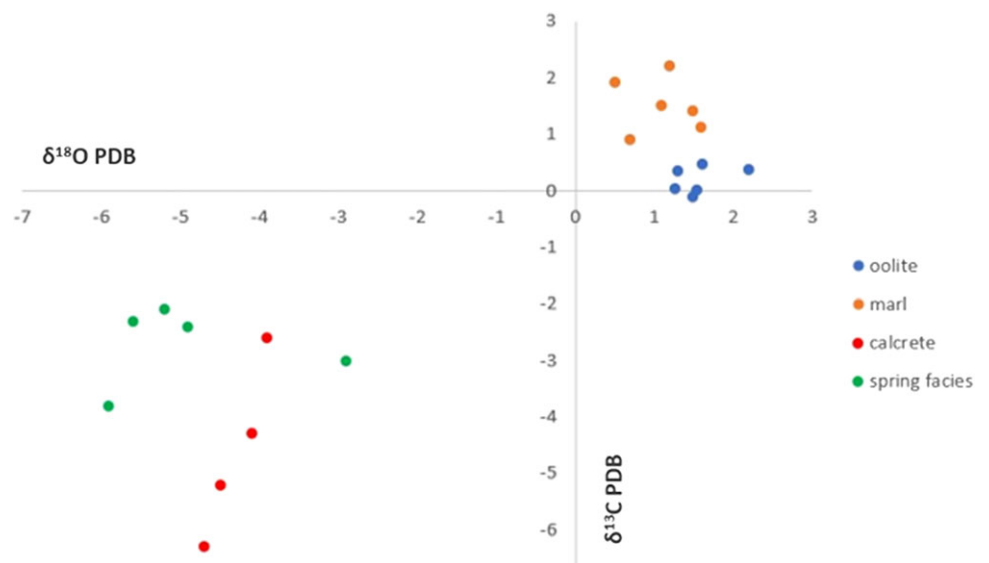
Figure 19. Carbon-oxygen isotope cross-plot for Ladye Bay oolites (Milroy 1998), Tea Green Marls (Blue Anchor Fm.) (Leslie *et al.* 1992) and calcrete-tufa-travertine (Leslie *et al.* 1993).

been observed by MET in Marsa Alam, Red Sea, Egypt (Tucker, 2003). Fine sediment in suspension can be carried great distances offshore, in low-density hypopycnal flows, travelling out over dense (saline) lake water for several km. When the clay is eventually deposited out of suspension, and this may be after several days, there will be a red clay layer on the lake floor, but *without* any associated coarser material, sand or pebbles. It is suggested that red chert nodules with no coarser clastic material are developed in these situations by water mixing (see below) within the yellow carbonates.

Soft-sediment deformation: Both red chert bands and dolomitic limestones show evidence of soft-sediment deformation. In a few places, the bedded dolomitic sediments are disturbed some distance away from the chert bands. The red bands themselves are conspicuously disturbed and disrupted. The shapes of the silicified bands, together with their presence as isolated nodules within the yellow dolomitic limestone, and with clasts of yellow sediment within the chert bands, suggest these sediments were ductile and easily deformable at the time. These observations are taken to imply that the lake was repeatedly an environment that was being disturbed both prior to and after formation of the red chert bands and nodules.

Syn-sedimentary deformation structures are common in lake sediments, especially those in active rift basins (e.g. Varejao *et al.* 2022). The overall depositional environment was an extensive lake basin in a desert/semi-arid location with an upland/hilly hinterland likely with contemporaneous active faulting. Soft-sediment deformation has been reported in the Blue Anchor Fm. elsewhere (Lavernock, Glamorgan; North Somerset coast) and in the overlying Rhaetic sediments (Mayall, 1983), related to seismic activity, although Simms (2007) attributed a deformed bed in the Cotham Member to meteorite impact.

Several processes common in such active lake–basin settings could be responsible for soft-sediment disturbances. Density inversion is a common cause of sediment deformation from Rayleigh-Taylor type instabilities, as in the sudden deposition of a relatively heavy sediment load onto a soft, muddy-sandy lake floor. Also, sediment compaction resulting in layered sediments with variable permeability can lead to later dewatering and transient trapping of water lenses with outbursts when these lenses suddenly

break through (Nichols *et al.* 1994). Additionally, a build-up of dissolved silica or silica gel (see later section) in the pore spaces of what would become the silicified rock could have resulted in a density contrast with underlying sediment, leading to instability. Seismic disturbance might also be related to nearby faults, and it is possible that the Clevedon fault itself was active at the time of lake deposition. Seismogenic shaking can trigger density instabilities, dewatering and liquefaction of unconsolidated sediments. These various mechanisms are not mutually exclusive (Nichols *et al.* 1994).

Possible dinosaur footprints at Clevedon would be no real surprise, since they are recorded in abundance in similar facies of similar age in Glamorgan (Tucker & Burchette, 1977; Lockley *et al.* 1996; Falkingham *et al.* 2022). Although there is only one almost convincing footprint, albeit with only 2 clear toes, but with a space where a third toe could have been, there are many features of sediment disturbance within/upon the particular footprint-bearing silicified red bed that could be attributed to 'dinoturbation'. Dinosaurs trampling across a soft-wet sediment surface, producing 'squelch' marks, were invoked by Tucker & Burchette (1977) and Falkingham *et al.* (2021) for the footprints at Barry and Penarth, South Wales. Two palaeobiologists familiar with footprints have visited the Clevedon site (Mike Benton, University of Bristol and Susie Maidment, BM(NH)) and both considered the evidence to be equivocal but not to be discarded. Deposition of the yellow dolomites would have been in shallow water, quite likely less than a metre, but periods of subaerial exposure would also be relatively frequent in this arid-zone location. There could well have been very shallow water, leading to subaerial exposure, after deposition of the red clastic material introduced by a flood, such that a dinosaur could then have walked across the newly deposited sediment layer.

The blue-grey marls are interpreted as dominantly lacustrine, for the most part low energy, at a time when only terrigenous clay was being provided to and being deposited within the basin, along with fine $CaCO_3$-dolomite being precipitated in the lake. Sedimentary features in the marl (Figures 11 a, b) do suggest occasional moderate to high-energy events (storms) causing erosion and disruption of the lake-floor sediments, reworking and some *in-situ* brecciation. Sediment deformation, disruption and brecciation can be explained as seismogenic, possibly linked to the adjacent major fault at
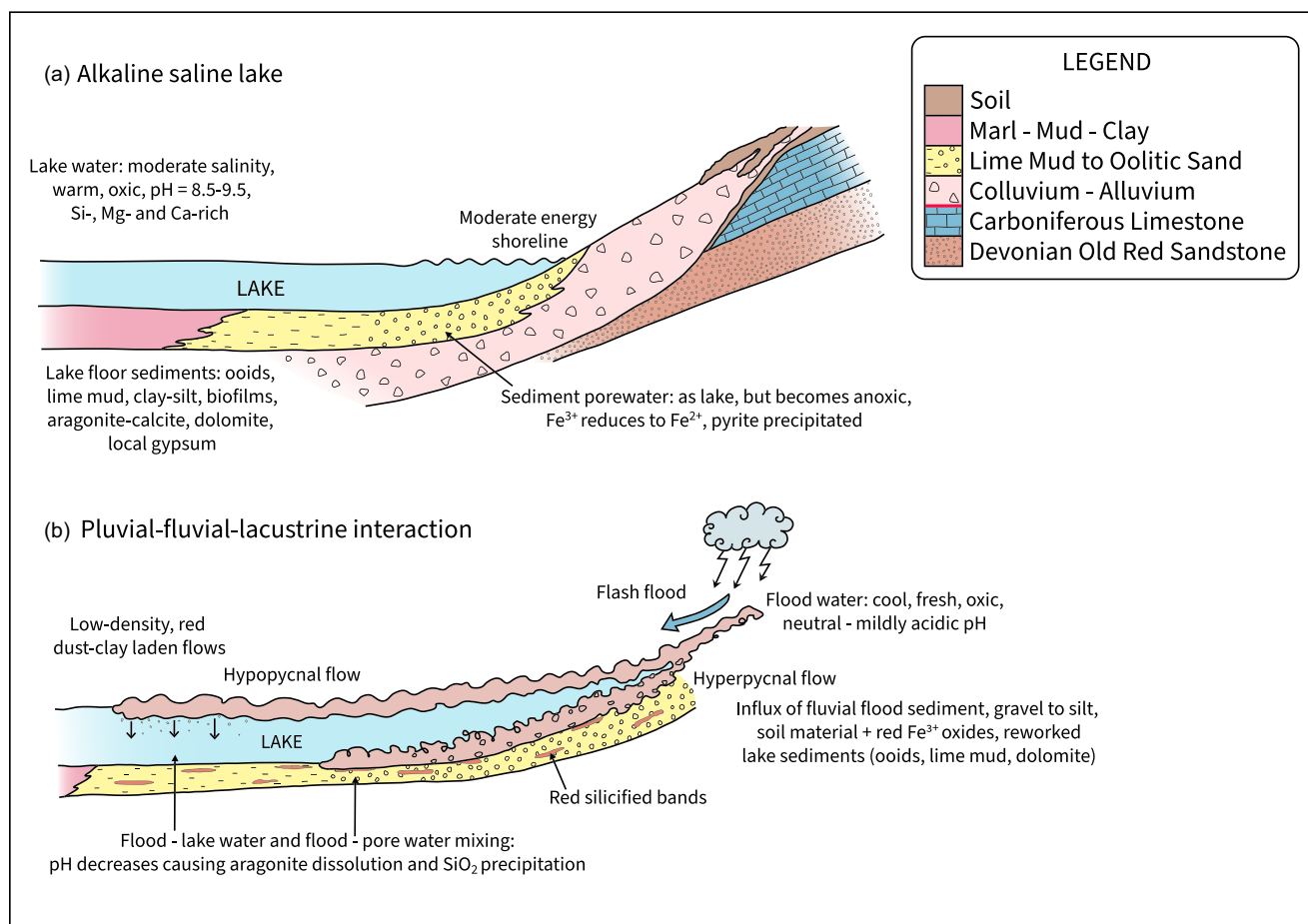
Figure 20. Schematic model for deposition and early diagenesis of the Triassic marginal lacustrine sediment, Bristol Channel Basin.

Clevedon. However, it should be noted that Mao *et al.* (2021) (and others, previously) proposed that the red MMG marls (and by extension the blue-grey marls) could be of aeolian dust origin, by comparison to the aeolian red clay on the Chinese Loess Plateau, in view of their grain size, micromorphology and geochemistry. Although there are many aspects of the MMG mudstones and marls which indicate the presence of a lake (e.g. Tucker, 1978), at Clevedon and Ladye Bay the oolite and cross-bedding (etc.) clearly demonstrate there was a lake here. The change from the typical red marls of the MMG to the blue-grey marls in the upper part (Blue Anchor Fm.) relates to increased humidity heralding the onset of marine conditions in the Rhaetic-Liassic.

The small outcrops of blue-grey marl near Clevedon Pier show all the features described from the 'classic' exposures of the Blue Anchor Fm. on the Glamorgan coast at Lavernock Point, Penarth and in Somerset at St Audrie's Bay (Mayall, 1981; Waters & Lawrence, 1987). This would indicate a younger age for the Clevedon yellow dolomites and Ladye Bay oolites than that suggested by Milroy & Wright (2000), although there is no biostratigraphic evidence available to substantiate this.

8.b. Early diagenesis

8.b.1. Dolomite and dolomitization
The dolomitization of the yellow carbonates is interpreted to be synsedimentary to very early diagenetic, on or just below the lake floor (Figure 20). The red and blue-grey marls of the Mercia Mudstone Group are both rich in dolomite, along with Mg-rich clays (sepiolite, palygorskite, corrensite) (Jeans, 1978; Leslie *et al.* 1993), indicating a high Mg/Ca ratio, high salinity and alkalinity. Occasional marine connections have been suggested for the MMG (as a source for halite at least, based on Br), which would also have provided Mg^{2+} ions. Dolomite is a common mineral in many arid-zone alkaline lakes, where the Mg/Ca ratio of the waters is relatively high and the Mg^{2+} contents are also high, and there is a significant degree of evaporation leading to increased salinity. Examples include the Coorong, South Australia (De Deckker, 2019), the Great Salt Lake, Utah (Dunham *et al.* 2020; Fang *et al.* 2023), Qaidam Lake in Tibet (Li *et al.* 2020), and lakes in Saskatchewan, Canada (Last *et al.* 2012) and western Siberia (Ovdina *et al.* 2020).

The former presence of pyrite (now oxidized) in the yellow carbonate sediment indicates that suboxic-anoxic conditions were established within the sediments soon after deposition. Organic matter would have been present, within biofilms covering the sediment surface in relatively quiet areas of the lake and in the sediment generated by planktic organisms in the lake, which then decomposed through aerobic heterotrophs to generate an anoxic environment for anaerobic fermentative bacteria and sulphate-reducing bacteria (SRB). Cyanobacteria and other photosynthesizing bacteria in the surface biofilm would have raised alkalinity, resulting in precipitation of $CaCO_3$. Furthermore, the presence of EPS (extracellular polymeric substances) and viruses within the

biofilms and in association with planktic bacteria can cause precipitation through their negative surface charge attracting Ca^{2+} and Mg^{2+} ions (Zhang *et al.* 2015; Perri *et al.* 2018; Al Disi *et al.* 2019; Paulo et al. 2020; Tucker, 2023b). In this Triassic lake, with saline alkaline water, a relatively high Mg/Ca ratio (Milroy & Wright, 2002) and a warm 'desert' temperature, aragonite would be expected to precipitate initially as lime mud in quiet areas and as ooids in moderate to high-energy shoreline locations. Such aragonite precipitates are widespread in the Great Salt Lake, Utah (Dunham *et al.* 2020). A higher temperature raises the SI (saturation index) of aragonite, and dolomite, considerably (5 × and 35 × from 25 to 40 °C, respectively (Paulo *et al.* 2020).

There are kinetic hindrances to direct 'primary' dolomite precipitation (Gregg *et al.* 2015; Tucker, 2023b). We therefore infer that initial aragonite precipitates were dolomitized, as in the Great Salt Lake (Dunham *et al.* 2020). The dolomite likely formed via a very high Mg calcite (VHMC) precursor, developing into disordered dolomite and then stoichiometric dolomite in time (c.f. dolomite 'maturing' across the Abu Dhabi sabkhas), with microbial activity and the presence of EPS and viruses promoting the process (Bontognali *et al.* 2010, 2014; Paulo et al. 2020; Tucker 2023b). Dolomite can form within the shallow subsurface suboxic-anoxic zone in the presence of SRB, lowering porewater pH, so promoting aragonite dissolution, and also leading to the precipitation of pyrite. The presence of SRB themselves, reducing the availability of SO_4^{2-}, is also likely to decrease ion-pairing with Mg^{2+}, potentially making it more available for replacement of Ca^{2+} in $CaCO_3$ (Vasconcelos & McKenzie, 1997; Van Lith *et al.* 2002; Bontognali *et al.* 2010). The presence of sulphide from SRB may have promoted dolomite formation by being adsorbed onto calcite faces, thereby reducing the energy required for dehydration of Mg^{2+}-water complexes (Zhang *et al.* 2012; Lu *et al.* 2018).

The hydration of Mg^{2+} ions is one of the main kinetic obstacles to dolomite precipitation generally. This can be reduced through the presence of dissolved sulphide (H_2S), hydrophilic amino acids, polysaccharides and carboxyl groups in EPS and on bacterial cell surfaces, and negatively-charged clay minerals such as illite and smectite (Qiu *et al.* 2017; Liu *et al.* 2019), all of which would be present in this alkaline lake environment and sediment porewater. One further factor lowering the dehydration barrier of a surface Mg^{2+}-water complex and promoting dolomite precipitation is the presence of hydrolyzed silica, $Si(OH)_4$ (Fang & Xu, 2022). This mechanism explains dolomite formation and distribution in the Great Salt Lake (Fang *et al.* 2023). Hydrolyzed silica is likely to have been in high concentration in this alkaline Triassic lake, with a higher $Si(OH)_4$ concentration at higher pH (>9; Tucker, 2023a). The silica would be derived from dissolution of wind-blown dust and suspended clay sediment in hypopycnal flows in the high pH lake water. The presence of hydrated silica and Mg^{2+} ions in lake water, along with a moderately high pH (8–9.5) can also lead to the precipitation of Mg-silicates, namely clays such as Mg-smectite, corrensite, sepiolite and palygorskite, which are present in the red and green Mercia Mudstone marls (Jeans, 1978; Mayall, 1981; Leslie *et al.* 1993).

8.c. Interpretations of stable isotope data

Values of the oolites and blue-grey marls are relatively close, being low positive in both $\delta^{13}C$ PDB and $\delta^{18}O$ PDB (Figure 19), and these are typical of lacustrine carbonates, including dolomites,

precipitated in alkaline saline lakes, such as those in East Africa (see Della Porta, 2015 and Guo *et al.* 2023 for reviews, and Zhao *et al.* 2023 for dolomite from Qaidam lake, Tibet). The isotope data are also similar to alkaline lake carbonates of the Pre-salt (Cretaceous), Santos Basin, Brazil (Wright & Barnett, 2017; Gomes *et al.* 2024). The low positive $\delta^{13}C$ PDB values of ooids and blue-grey marl do not indicate any significant extreme microbial or meteoric water influence on carbonate precipitation; rather, they reflect an overall equilibrium between dissolved inorganic carbon in the lake water and atmospheric CO_2 (Leng & Marshall, 2004). The positive $\delta^{18}O$ PDB signatures are consistent with significant evaporation, driving off the lighter ^{16}O. In contrast, Triassic calcretes and travertine-tufa from Glamorgan have low to moderately negative signatures in both $\delta^{13}C$ PDB and $\delta^{18}O$ PDB. These are typical values for non-marine, pedogenic – spring deposits with fluids of meteoric origin and some microbial influence (Andrews *et al.* 1993; Andrews, 2006).

8.d. Silicification

One hypothesis for the formation of the red silicified bands and nodules is by ingress of meteoric water, plausibly introduced by flash floods into the lacustrine environment. The water transporting coarse terrigenous sediment (hyperpycnal flows) and that with suspended red clay (hypopycnal flows) would have had a markedly different composition from that of the lake and sediment pore waters. As discussed above, from the mineralogy of the lacustrine carbonates and clays and the local presence of evaporites in the succession, alkaline, saline waters with a relatively high Mg content and moderately high pH are inferred, as has been documented for the Mercia Mudstone Group sediments generally (Jeans, 1978; Talbot *et al.* 1994; Wright & Sandler, 1994; Milroy & Wright, 2000). Such alkaline water is expected to contain significant amounts of silica in solution, in a hydrolyzed form, $Si(OH)_4$, in view of the increased solubility of silica at high pH (Bustillo, 2010; Tucker, 2023a). The storm water entering the shallow lake would be fresh-meteoric, with low salinity and near-neutral pH. We infer that the lake was supplied with low-silica water and that the silica concentration increased in the lake through a combination of evaporation and increased pH governed by the biology and chemistry as described earlier, as well as dissolution of clays imported in suspension or in wind-blown dust. Silica contents could reach a high enough concentration such that a colloid or gel could form. The presence of very high amounts of silica in gel form could also account for sinking of the domains that would eventually become silicified rock into the underlying sediment and their ductile character. Silicification might then be triggered when the Si content reached a threshold governed by the meteoric water influx with lowering of pH and evaporation. Suitable conditions for triggering might be expected to develop following prolonged drought and then a sudden influx of low-pH freshwater.

That the silicified beds are red and the sediment was prone to soft-sediment deformation indicates that the silicification is a very early event. As noted above, the yellow carbonate sediment became anoxic in the shallow subsurface and pyrite was precipitated. In modern shallow-marine-lacustrine environments, this takes place from a few mm to 10s of cm below the sea/lake floor as a result of the decomposition of organic matter and consumption of oxygen. Fe-oxide particles (red dust, clay) deposited out of suspension on

the lake floor would have been dissolved in anoxic porewaters on shallow burial and then re-precipitated as pyrite, if not preserved within the chert/silica gel before this. Thus, the preservation of the red colour of the silicified layers and nodules is significant, indicating very early precipitation of silica to form a tight, low porosity-permeability rock with the Fe-oxide particles protected from reduction.

The silicification is in the form of precipitation of quartz crystals, as a micro- to mega- quartz cement within pore spaces within the sediment, as well as within the voids once occupied by ooids; some replacement of the fine-grained lime mud matrix in the red sediment could also have occurred. With the original aragonite mineralogy of the ooids, the influx of meteoric water would have favoured their dissolution. The partial fracture of the outer lamellae of ooids (Figures 15 a–d) and then quartz cementation, also indicate extremely early silica precipitation. The growth of the micro- to mega- quartz crystals could have taken place within an initial precipitate of silica gel.

Silicification of lacustrine carbonates has been reported from several other formations, notably the Tertiary of the Madrid Basin, Spain (e.g., Bustillo *et al.* 2002), the Aptian Pre-salt of the South Atlantic Basins, offshore Brazil and Angola (Wright & Barnett 2015; Pereira *et al.* 2023; Gomes *et al.* 2024) and the Permian Fengcheng Formation, China (Yu *et al.* 2024). With the Pre-salt, a huge alkaline lake developed during the initial opening of the South Atlantic, freshening of lake waters during phases of a more humid climate is thought to have triggered silicification of carbonates through decreasing alkalinity and pH; however, some silicification is related to hydrothermal fluids (Teboul *et al.* 2019; Lima *et al.* 2020), as is that in the Fengcheng Fm. (Yu *et al.* 2024).

The initial precipitation of the hydrolyzed silica in solution in the lake water through freshening and reduction of pH could have been in the form of a precursor amorphous silica or a silica gel. This process has been described from some alkaline-saline East African lakes, where gels of Na and Mg silicates are also forming, with the silicon and other ions leached from volcanic rocks in the hinterland (Eugster & Jones, 1968; Renaut *et al.* 2002; Renaut *et al.* 2021; Raudsepp *et al.* 2023). Siliceous precipitates here include magadiite, a metastable hydrated sodium silicate, which converts to chert in a relatively short time (Owen *et al.* 2019). The formation of gels as a precursor to silica has been invoked for the Aptian Pre-salt of the South Atlantic basins (Wright, 2022; Wright & Barnett, 2015), with precipitation, again, taking place when pH is lowered, as through freshwater input. Evaporation then leads to Mg-silicate formation, notably stevensite and kerolite. An analogous process producing gelatinous opaline chert is occurring in several lakes in South Australia (Peterson & von der Borch, 1965; Ambrose & Flinn, 1981), attributed to the mixing of ground water and lake water during falling lake level, and/ or seasonal pH changes.

Silicified sediments and soils forming *silcretes* develop through pedogenesis in the shallow subsurface of soil profiles and somewhat deeper at the groundwater table (Ambrose & Flinn, 1981; Ullyott & Nash, 2016; Taylor & Eggleton, 2017). These are mostly composed of microquartz, but with coarser fabrics in vugs and there are commonly relics of plant roots present in the form of canals and tubes. These deposits can be a metre or more thick and may be autobrecciated. In the case of the Triassic red silicified sediments here, generally thin layers and discrete nodules of chert within 'normally'-deposited carbonates, there are no textures suggesting pedogenesis, and no evidence of the former presence of

rootlets. Chalcedonic quartz, typical of hydrothermal silica (Lima *et al.* 2020), is also absent. However, a key observation which could support a precursor high silica concentration gel as an intermediate step to complete silicification is the ductile behaviour of the domains that eventually became hard silicified rock. These bands and layers have plastic shapes and became involved in soft-sediment deformation. In fact, early syn-sedimentary deformation is common in silicified sediments generally (e.g. Gimenez-Monsant *et al.* 1999, Eocene of Spain), including the Pre-salt of Brazil (Pereira *et al.* 2023). Such features could reflect the effects of density contrasts between a gel of hydrolyzed silica, micro- mega- quartz, and the host dolomite mud.

Although we conclude that silicification is very early and related to syn-sedimentary pore-fluid mixing, there are records of extensive silicification in the Mendips area within the Dolomitic Conglomerate near East Harptree and also in the Lower to Middle Jurassic coarse bioclastic limestones (Brockley Down Limestone) on the north side of the Mendip Hills (Simms, 1995; King, Strategic Stone Study, 2011). This silicification is more pervasive stratigraphically and is likely related to the hydrothermal fluids involved in the Mendip Pb–Zn mineralization, thought to be of Jurassic age (Simms, 1995), and contrasts with the more bed-bound localized silicification of the red chert bands and nodules at Clevedon and their evidence for a very early diagenetic origin.

The silicified nodules present within the yellow dolomites lower in the succession at Clevedon (Figure 10 a, b) are similar to nodules noted by Milroy (1998) in his units 1 and 2 at Ladye Bay. The overall shape and 'cauliform' external surface suggest they are replaced anhydrite nodules, which may well have formed from replacement of cm-scale gypsum crystals precipitated within the sediment. Such sulphates are common in arid-zone littoral lacustrine and high inter-supra-tidal marine facies and are typical of sabkha facies generally. Similar facies have been described from the Marginal Triassic of Glamorgan by Tucker (1978) and Leslie *et al.* (1993). These nodules, also referred to as 'potato stones', are similar in external shape to Bristol diamonds (Tucker, 1976), with some also having a central cavity containing large megaquartz crystals, the feature of the 'diamond' geodes. The 'full-bodied' shape/uncompacted nature of the nodules indicates an early timing for their silicification and this probably occurred through freshwater ingress in a similar manner to the formation of the red silicified bands and nodules higher in the succession.

8.e. Later diagenesis: burial and uplift

The Triassic sediments were buried to a depth probably in excess of 800 m until regional uplift began in the early Cenozoic. During this time, fracturing and faulting of the Triassic sediments took place in response to regional stresses related to opening of the Central Atlantic and formation of Mesozoic basins, such as the Wessex Basin to the southeast, with movement on reactivated Variscan and younger faults (Cosgrove *et al.* 2021). Apart from some pressure dissolution planes, stylolites and calcite veins, the main post-Triassic event was the passage of hydrothermal fluids up the Clevedon Pier fault and associated fractures and consequent precipitation of Pb-Cu sulphides and baryte there in the fault breccia and adjacent porous yellow dolomite (Ixer *et al.* 1993). Galena (mm-cm scale patches) is conspicuous in fractures within the yellow dolomite at Clevedon, as is baryte, notably within the Dolomitic Conglomerate and fault breccia, but it is also disseminated as sub-mm particles within the yellow dolomite, as seen in SEM-EDS maps (Figure 18 a).

The yellow colour of the Triassic dolomite beds is attributed to the oxidation of disseminated pyrite and replacement by goethite-limonite. This could have taken place during moderate to deep burial if the porewaters were oxic, as is the case with many deeper groundwaters as a result of the extensive microbiota occurring in the subsurface and the generation of dark oxygen there (Ruff *et al.* 2023). However, oxidation of pyrite would also have taken place much later during Cenozoic uplift on interaction with surface-derived oxic groundwaters. In fact, many carbonate rocks in the UK, from the Permian, Triassic and Jurassic, are a buff-yellow-honey colour at outcrop, but a dark grey colour, even blue, in the shallow subsurface as a result of the presence of original organic matter and pyrite (Tucker, 2023c). During this late phase of exhumation and weathering of the Clevedon yellow dolomites in the last few million to few 10s of 1000s years, it is likely that the black Mn-oxide particles and dendrites also formed. Mn would be released from organic matter, clays and pyrite in the highly oxic near-surface groundwaters. The oxidation (Liesegang) rings would also have formed at this time from episodic migration of oxic chemical fronts (Ashley, 2014).

8. Conclusions

Upper Triassic lacustrine yellow dolomites of the Mercia Mudstone Group in the Bristol Channel basin in the vicinity of Clevedon were deposited in the marginal area of an alkaline saline lake at a time of extreme aridity. Conditions were conducive to the precipitation of aragonite-HMC lime mud and growth of biofilms in low-energy areas and ooids along agitated, wave-dominated shorelines. Anoxic conditions soon developed during shallow burial and pyrite precipitated. Conspicuous red chert beds, bands and nodules within the yellow dolomites were the result of silicification, which in some cases occurs within beds of more clastic-rich sediment, and in others, forms 'random' nodules and discontinuous bands. The silicification is attributed to occasional flash floods providing freshwater and coarse to fine terrigenous material from the hinterland to the lake in hyperpycnal flows, along with hypopycnal flows transporting suspended Fe-rich (red) dust. The input of near-neutral pH meteoric water resulted in local dissolution of aragonitic ooids and its interaction with the alkaline lake-sediment pore water led to the precipitation of silica to form the chert beds, bands and nodules, with a red colour from the finely disseminated Fe-oxide. Oomolds and associated inter-grain pores were filled with drusy quartz. The silicified bands show a range of soft-sediment deformation structures which may be related to the formation of silica gel as a precursor to the chert, inducing density contrasts within the sediment, along with dewatering or seismic activity.

The depositional-diagenetic model (Figure 20) deduced for these Triassic carbonate-chert rocks involving fluid mixing and water redox-pH-temperature changes resulting in mineral dissolution, precipitation and replacement, is applicable to many other arid-zone cases of pluvial-fluvial-lacustrine interaction reported in the geological record. Data from field observations, petrography-SEM and chemical analyses combine to enable the model to be presented.

References

Al Disi ZZA, Bontognali TRR, Jaoua S, Attia E, Al Saad Al-Kuwari H and Zouari, N (2019) Influence of temperature, salinity and Mg^{2+}:Ca^{2+} ratio on microbially mediated formation of Mg-rich carbonates by *Virgibacillus* strains isolated from a sabkha environment. *Nature Scientific Reports* **9**, 19633. https://doi.org/10.1038/s41598-019-56144-0

Ambrose GJ and Flinn RB (1981) A regressive Miocene lake system and silicified strandlines in northern South Australia: implications for regional stratigraphy and silcrete genesis. *Journal of the Geological Society of Australia* **28**, 81–94.

Andrews JE (2006) Palaeoclimatic records from stable isotopes in riverine tufas: Synthesis and review. *Earth Science Reviews* **75**, 85–104.

Andrews JE, Riding R and Dennis PF (1993) Stable isotopic compositons of Recent freshwater cyanobacterial carbonates from the British Isles: local and regional environmental controls. *Sedimentology* **40**, 303–314.

Andrews SD and Hartley AJ (2015) The response of lake margin sedimentary systems to climatically driven lake level fluctuations: Middle Devonian, Orcadian Basin, Scotland. *Sedimentology* **62**, 1693–1716. doi: 10.1111/sed.12200

Ashley RW (2014) Liesegang rings in lacustrine Triassic limestone of Clevedon, North Somerset. *Proceedings of the Bristol Naturalists' Society* **74**, 8–15.

Ashley RW, Wright VP and Marriott SB (2024) The Geology of the Clevedon Coast. In *The Geology of the Bristol Region* (ed Lavis S). London: Guide No. 78, Geologists' Association.

Baranyi V, Miller CS, Ruffell A, Hounslow MW and Kurschner WM (2019) A continental record of the Carnian Pluvial Episode (CPE) from the Mercia Mudstone Group (UK): palynology and climatic implications. *Journal of the Geological Society of London* **176**, 149–166.

Birgenheier LP, Vanden Berg MD, Plink-Björklund P, Gall RD, Rosencrans E, Rosenberg MJ, Toms LC and Morris J (2020) Climate impact on fluvial-lake system evolution, Eocene Green River Formation, Uinta Basin, Utah, USA. *Geological Society of America Bulletin* **132**, 562–587. doi: 10.1130/B31808.1.

Bontognali TRR, McKenzie JA, Warthmann RJ and Vasconcelos C (2014) Microbially influenced formation of Mg-calcite and Ca-dolomite in the presence of exopolymeric substances produced by sulphate-reducing bacteria. *Terra Nova* **26**, 72–77.

Bontognali TRR, Vasconcelos C, Warthmann RJ, Bernasconi SM, Dupraz C, Strohmenger CJ and McKenzie JA (2010) Dolomite formation within microbial mats in the coastal sabkha of Abu Dhabi (United Arab Emirates). *Sedimentology* **57**, 824–844.

Bustillo MA (2010) Silicification of continental carbonates. In *Carbonates in Continental Settings: Processes, Facies and Applications* (eds Alonso-Zarza A and Tanner LH), pp. 153–174. Oxford: Elsevier.

Bustillo MA, Arribas ME and Bustillo M (2002) Dolomitization and silicification in low-energy lacustrine carbonates (Paleogene, Madrid Basin, Spain). *Sedimentary Geology* **151**, 107–126.

Chadwick RA and Evans DJ (1995) The timing and direction of Permo-Triassic extension in Southern Britain. *Geological Society of London Special Publication* **91**, 161–192.

Chudasama B, Porwal A, González-Álvarez I, Thakura S, Wilde A and Kreuzer OP (2018) Calcrete-hosted surficial uranium systems in Western Australia: Prospectivity modeling and quantitative estimates of resources.

Part 1 – Origin of calcrete uranium deposits in surficial environments: A review. *Ore Geology Reviews* **102**, 906–9.

Clemmensen LB, Kent DV and Jenkins FA (1998) A late Triassic lake system in East Greenland: facies, depositional cycles and paleoclimate. *Palaeogeography, Palaeoclimatology, Palaeoecology* **1401**, 135–159.

Cosgrove J, Morgan TO and Ghail R (2021) The deformation history of southern England and its implications for ground engineering in the London Basin. *Quarterly Journal of Engineering and Hydrogeology* **55**. doi: 10.1144/qjegh2020-144.

De Deckker P (2019) Groundwater interactions control dolomite and magnesite precipitation in saline playas in the Western District Volcanic Plains of Victoria, Australia. *Sedimentary Geology* **380**, 105–126.

Della Porta G (2015) Carbonate buildups in lacustrine, hydrothermal and fluvial settings: comparing depositional geometry, fabric types and geochemical signature. *Geological Society of London Special Publication* **418**, 17–68.

Dunham EC, *et al* (2020) An ecological perspective on dolomite formation in the Great Salt Lake. *Frontiers in Earth Sciences* **8**, 24. doi: 10.3389/feart.2020.00024

Eardley AJ (1938) Sediments of the Great Salt Lake, Utah. *Bulletin American Association of Petroleum Geologists* **22**, 1305–1411.

Enos P and Sawatsky LH (1981) Pore networks in Holocene carbonate sediments. *Journal of Sedimentary Petrology* **51**, 961–985.

Eugster HP and Jones BF (1968) Gels composed of sodium aluminium silicate, Lake Magadi, Kenya. *Science* **161**(3837), 160–163.

Falkingham PL, Maidment SCR, Lallensack JN, Martin JE, Suan G, Cherns L, Howells C and Barrett PM (2022) Late Triassic dinosaur tracks from Penarth, South Wales. *Geological Magazine* **159**, 821–832. doi: 10.1017/S0016756821001308.

Fang Y, Hobbs F, Yang Y and Xu H (2023) Dissolved silica driven dolomite precipitation in the Great Salt Lake, Utah and its implications for dolomite-forming environments. *Sedimentology* **70**, 1328–1347.

Fang Y and Xu H (2022) Dissolved silica-catalysed disordered dolomite precipitation. *American Mineralogist* **107**, 443–452.

Gall RD, Birgenheier LP and Van den Berg MD (2017) Highly seasonal and perennial fluvial facies: implications for climatic control on the Douglas Creek and Parachute Creek Members, Green River Formation, southeastern Uinta Basin, Utah, U.S.A. *Journal of Sedimentary Research* **87**, 1019–1047.

Gimenez-Montsant J, Calvet F and Tucker ME (1999) silica diagenesis in Eocene shallow-water platform carbonates, southern Pyrenees. *Sedimentology* **46**, 969–984.

Gomes JPB, Bunevich RB, Sartorato ACL, Tedeschi, LR, Tonietto SN, Tucker ME and Whitaker F (2024) Early diagenetic evolution based on petrography and stable isotope analysis in the Barra Velha Formation of the Brazilian Pre-salt. *The Depositional Record* 1–25. doi: 10.1002/dep2.288.

Goodwin B (1982) Calculated uranium solubility in ground water; implications for radioactive waste disposal. *Canadian Journal of Chemistry* **60**, 1759–1766.

Gregg JM, Bish DL, Kaczmarek SE and Machel HG (2015). Mineralogy, nucleation and growth of dolomite in the laboratory and sedimentary environment: a review. *Sedimentology* **62**, 1749–1769. doi: 10.1111/sed.12202

Guo P, Wen H, Li C, He H and Sanchez-Roman M (2023) Lacustrine dolomite in deep time: What really matters in early dolomite formation and accumulation? *Earth Science Reviews* **246**, 104575.

Hearn PP and Sutter JF (1985) Authigenic potassium feldspar in Cambrian carbonates: Evidence of Alleghenian brine migration. *Science* **228**, 1529–1531.

Howard AS, Warrington G, Ambrose K and Rees JG (2008) A formational framework for the Mercia Mudstone Group (Triassic) of England and Wales. *British Geological Survey Research Report*: RR/08/04.

Howson MP, Tucker ME and Whitaker FF (2022) Rare preservation of Triassic pedorelicts with biogenic traces reworked from a hot semi-arid upland palaeoenvironment at Portishead, SW England. *Proceedings of the Geologists' Association* **133**, 572–588. doi: 10.1016/j.pgeola.2022.07.003

Husein SS, Fraser A, Roberts GG and Bell R (2022) New insights into the stratigraphic evolution of SW Britain: implications for Triassic salt and hydrocarbon prospectivity. *Petroleum Geoscience* **29**(2). doi: 10.1144/petgeo2022-051

Ixer RA, Pattrick RAD and Starkey RE (1993) Lead-zinc-copper-arsenic-baryte mineralization from Clevedon, near Bristol. *Journal Russell Society* **5**, 23–30.

Jeans CV (1978) The origin of the Triassic clay assemblages of Europe with special reference to the Keuper Marl and Rhaetic of parts of England. *Philosophical Transactions of the Royal Society Series A: Mathematical & Physical Science* **289**, 549–639.

King A (2011) *Strategic Stone Study: A Building Stone Atlas of Avon*. English Heritage.

Last FM, Last WM and Halden NM (2012) Modern and late Holocene dolomite formation: Manito Lake, Saskatchewan, Canada. *Sedimentary Geology* **281**, 222–237.

Leng MJ and Marshall JD (2004) Palaeoclimate interpretation of stable isotope data from lake sediment archives. *Quaternary Science Reviews* **23**, 811–831.

Leslie AB, Spiro B and Tucker ME (1993) Geochemical and mineralogical variations in the upper Mercia Mudstone Group (Late Triassic), southwest Britain: correlation of outcrop sequences with borehole geophysical logs. *Journal of the Geological Society London* **150**, 67–75.

Leslie AB and Tucker ME (1995) Discussion on a hydrogeological model for the early diagenesis of Late Triassic alluvial sediments. *Journal of the Geological Society of London* **152**, 732–734.

Leslie AB, Tucker ME and Spiro B (1992). A sedimentological and stable isotopic study of travertines and associated sediments within the Upper Triassic lacustrine limestones, S. Wales. *Sedimentology* **39**, 613–629.

Li J, Zhu L, Lia M, Wang J and Ma Q (2020) Origin of modern dolomite in surface lake sediments on the central and western Tibetan Plateau. *Quaternary International* **544**, 65–75.

Lima BEM, Tedeschi LR, Pestilho ALP, Santos RV, Vazquez JC, Guzzo JVP and De Ros LF (2020) Deep-burial hydrothermal alteration of the Pre-Salt carbonate reservoirs from northern Campos Basin, offshore Brazil: Evidence from petrography, fluid inclusions, Sr, C and O isotopes. *Marine & Petroleum Geology* **113**, 104143.

Liu D, Xu Y, Papineau D, Yu N, Fan Q, Qiu X and Wang H (2019) Experimental evidence for abiotic formation of low-temperature proto-dolomite facilitated by clay minerals. *Geochimica Cosmochimica Acta* **247**, 83–95.

Lockley MG, King M, Howe S and Sharp T (1996) Dinosaur tracks and other archosaur footprints from the Triassic of South Wales. *Ichnos: An International Journal of Plant & Animal* **5**, 23–41.

Lowenstein TK and Risacher F (2009) Closed basin brine evolution and then influence of Ca-Cl inflow waters: Death Valley and Bristol Dry Lake California, Qiadam Basin China and Salar de Atacama, Chile. *Aquatic Geochemistry* **15**, 71–94.

Lu Y, Sun X, Xu H, Konishi H, Lin Z and Xu L (2018). Formation of dolomite catalyzed by sulfate-driven anaerobic oxidation of methane: mineralogical and geochemical evidence from the northern South China Sea. *American Mineralogist* **103**, 720–734. doi: 10.2138/am-2018-6226.

Mann SJ and Amos KJ (2022): Sedimentology and geomorphology of Lake Yamma Yamma - A long-lived structurally controlled playa lake of the Lake Eyre Basin, Australia. *Transactions of the Royal Society of South Australia*. doi: 10.1080/03721426.2022.2027649

Mao, X., Liu, X. and Zhou, X. (2021) Permo-Triassic aeolian red clay of southwestern England and its palaeoenvironmental implications. *Aeolian Research* **52**, 100726.

Mayall ME (1981) The Late Triassic Blue Anchor Formation and the initial Rhaetian marine transgression in south-west Britain. *Geological Magazine* **118**, 374–381.

Mayall ME (1983) An earthquake origin for synsedimentary deformation in a late Triassic (Rhaetian) lagoonal sequence, southwest Britain. *Geological Magazine* **120**, 613–622.

McKie T and Williams B (2009) Triassic palaeogeography and fluvial dispersal across the northwest European basins. *Geological Journal* **44**, 711–741.

Milroy P (1998) *Palaeoenvironmental analysis of the Mercia Mudstone Group (Upper Triassic) of the Severn Basin and Bristol Channel Region, Southwest Britain*. Unpublished PhD Thesis, University of Bristol, Bristol, UK, 292 pp.

Milroy P and Wright VP (2000) A highstand oolitic sequence and associated facies from a Late Triassic lake basin, south-west England. *Sedimentology* **47**, 187–209.

Milroy P and Wright VP (2002) Fabrics, facies control and diagenesis of lacustrine ooids and associated grains from the Upper Triassic, southwest England. *Geological Journal* **37**, 35–53.

Milroy P, Wright VP and Simms MJ (2019) Dryland continental mudstones: Deciphering environmental changes in problematic mudstones from the Upper Triassic (Carnian to Norian) Mercia Mudstone Group, south-west Britain. *Sedimentology* **66**, 2557–2589. doi: 10.1111/sed.12626

Nichols RJ, Sparks RSJ and Wilson CJN (1994) Experimental studies of the fluidisation of layered sediments and the formation of fluid escape structures. *Sedimentology* **41**, 233–253.

North CP (1988) *Structure and Sedimentology of the Mercia Mudstone Group (Upper Triassic), Severn Estuary Region, Southwest Britain*. Unpublished PhD Thesis, University of Bristol, Bristol, UK, 346 pp.

Ovdina E, Strakhovenko V and Solotchina E (2020) Authigenic carbonates in the water–biota–bottom sediments' system of small lakes (South of Western Siberia). *Minerals* **10**, 552.

Owen RB, Renaut RW, Muiruri VM, Rabideaux NM, Lowenstein TK, McNulty EP, Leet K, Deocampo D, Luo S, Deinoh AL, Cohen A, Sierj MJ, Campisanol C, Shenm C-C, Billingsleyi A, Mbuthiao A and Stockheckep M (2019) Quaternary history of the Lake Magadi Basin, southern Kenya Rift: Tectonic and climatic controls. *Palaeogeography, Palaeoclimatology, Palaeoecology* **518**, 97–118.

Paulo C, McKenzie JA, Raoof B, Bollmann J, Fulthorpe R, Strohmenger CJ and Dittrich M (2020) Organomineralization of proto-dolomite by phototrophic microbial mat extracellular polymeric substances: Control of crystal size and its implication for carbonate depositional systems. *American Journal of Science* **320**, 72–95.

Pereira TP, Terra S, da Silva DR, Pires GLC and Ribeiro A (2023) Distribution of silicification intervals throughout the Barra Velha and Itapema formations: Host rock controls and chronology of silica precipitation (Pre-Salt, Santos Basin, Brazil). *Journal of South American Earth Sciences* **128**, 14446.

Perri E, Tucker ME, Słowakiewicz M, Whitaker FF, Bowen L and Perrotta I (2018) Carbonate and silicate biomineralization in a hypersaline microbial mat (Mesaieed Sabkha, Qatar): roles of bacteria, EPS and viruses. *Sedimentology* **65**, 1213–1245.

Peterson MNA and von der Borch CC (1965) Chert: modern inorganic deposition in a carbonate-precipitating locality. *Science* **149**, 1501–1503.

Popp BN and Wilkinson BH (1983) Holocene lacustrine ooids from Pyramid Lake, Nevada. In *Coated Grains*, pp. 142–153. Springer.

Porter RJ and Gallois RW (2008) Identifying fluvio–lacustrine intervals in thick playa-lake successions: an integrated sedimentology and ichnology of arenaceous members in the mid–late Triassic Mercia Mudstone Group of south-west England, UK. *Palaeogeography, Palaeoclimatology, Palaeoecology* **270**, 381–398.

Qiu X, Wang H, Yao Y and Duan Y (2017) High salinity facilitates dolomite precipitation mediated by *Haloferax volcanii* DS52. *Earth and Planetary Science Letters* **472**, 197–205.

Raudsepp MJ, Wilson S and Morgan B (2023) Making salt from water: the unique mineralogy of alkaline lakes. *Elements* **19**, 22–29.

Reijmer JJG, Blok CM, El-Husseiny A, Kleipool LM, Hogendorp YCK and Alonso-Zarza AM (2020) Petrophysics and sediment variability in a mixed alluvial to lacustrine carbonate system (Miocene, Madrid Basin, Central Spain). *The Depositional Record*. doi: 10.1002/dep2.158

Renaut RW, Jones B, Tiercilin J-J and Tarits C (2002) Sublacustrine precipitation of hydrothermal silica in rift lakes: evidence from Lake Baringo, central Kenya Rift Valley. *Sedimentary Geology* **148**, 235–257.

Renaut RW, Owen RB, Lowenstein TK, de Cort G, McNulty E, Scott JJ and Mbuthia A (2021) The Role of Hydrothermal Fluids in Sedimentation in Saline Alkaline Lakes: Evidence from Nasikie Engida, Kenya Rift Valley. *Sedimentology* **68**, 108–134.

Ruff SE, *et al* (2023) Hydrogen and dark oxygen drive microbial productivity in diverse groundwater systems. *Nature Communications* **14**, 3194.

Shettima B, Kyari AM, Aji MM and Adams FD (2018) Storm and tide influenced depositional architecture of the Pliocene-Pleistocene Chad Formation, Chad Basin (Bornu Sub-basin) NE Nigeria: A mixed fluvial, deltaic, shoreface and lacustrine complex. *Journal of African Earth Sciences* **143**, 309–320.

Simms MJ (1995) The geological history of the Mendip Hills and their margins. *Proceedings of the Bristol Naturalists' Society* **55**, 113–134.

Simms MJ (2007) Uniquely extensive soft sediment deformation in the Rhaetian of the UK: Evidence for earthquake or impact? *Palaeogeography, Palaeoclimatology, Palaeoecology* **244**, 407–423.

Singewald JT and Milton C (1929) Authigenic feldspar in limestone at Glens Falls, New York. *Geological Society of America Bulletin* **40**, 463–468.

Smedley PL and Kinniburgh DG (2023) Uranium in natural waters and the environment: distribution, speciation and impact. *Applied Geochemistry* **148**, 105534.

Smoot JP (1991) Sedimentary facies and depositional environments of early Mesozoic Newark Supergroup basins, eastern North America. *Palaeogeography, Palaeoclimatology, Palaeoecology* **84**, 369–423.

Stanley DM and Wilkin RT (2019) Solution equilibria of uranyl minerals: role of common ground water ions calcium and carbonate. *Journal of Hazardous Materials* **377**, 315–320.

Talbot MR, Holm K and Williams MAJ (1994) Sedimentation in low gradient desert margin systems - a comparison of the late Triassic of northwest Somerset (England) and the late Quaternary of east-central Australia. In *Paleoclimate and Basin Evolution of Playa Systems* (ed Rosen MR), *Geological Society of America Special Paper 289*, pp. 97–117.

Tanner LH (2000) Palustrine–lacustrine and alluvial facies of the (Norian) Owl Rock Formation (Chinle Group), Four Corners region, southwestern U.S.A.: implications for late Triassic paleoclimate. *Journal of Sedimentary Research* **70**, 1280–1289.

Taylor G and Eggleton RA (2017) Silcrete: an Australian perspective. *Australian Journal of Earth Sciences* **64**, 987–1016. doi: 10.1080/08120099.2017.1318167

Teboul P-A, Durlet C, Girard J-P, Dubois L, San Miguel G, Virgone A, Gaucher EC and Camoin G (2019) Diversity and origin of quartz cements in continental carbonates: Example from the Lower Cretaceous rift deposits of the South Atlantic margin. *Applied Geochemistry* **100**, 22–41.

Tucker ME (1976) Quartz-replaced anhydrite nodules ('Bristol Diamonds') from the Triassic of the Bristol district. *Geological Magazine*, **113**, 569–579.

Tucker ME (1977) The marginal Triassic deposits of South Wales: continental facies and palaeogeography. *Geological Journal* **12**, 169–88.

Tucker ME (1978) Triassic lacustrine sediments from South Wales: shore-zone elastics, evaporites and carbonates. In: *Modern and Ancient Lake Sediments* (ed Matter A and Tucker ME), *International Association of Sedimentologists Special Publication 2*, pp. 205–224.

Tucker ME (2003) Mixed clastic-carbonate cycles and sequences: Quaternary of Egypt and Carboniferous of England. *Geologia Croatica* **56**, 19–37.

Tucker ME (2023a) Chapter 9 Cherts and siliceous sediments. In *Sedimentary Petrology* (eds Tucker ME and Jones SJ), pp. 401–417. Chichester: John Wiley.

Tucker ME (2023b) Chapter 4 Carbonate sediments: limestones and dolomites. In *Sedimentary Petrology* (eds Tucker ME and Jones SJ), pp. 204–325. Chichester: John Wiley.

Tucker ME (2023c) Blue Bath Stone: the real colour of Bath Oolite (Middle Jurassic, England). *Journal of the Bath Geological Society* **41**, 9–11.

Tucker ME and Burchette TP (1977) Triassic dinosaur footprints from South Wales: their context and preservation. *Palaeogeography, Palaeoclimatology, Palaeoecology* **22**, 195–208.

Ullyott JS and Nash DJ (2016) Distinguishing pedogenic and non-pedogenic silcretes in the landscape and geological record. *Proceedings of the Geologists' Association* **127**, 311–319.

Van Lith Y, Vasconcelos C, Warthmann R, Martins JCF and McKenzie JA (2002) Bacterial sulfate reduction and salinity: two controls on dolomite precipitation in Lagoa Vermelha and Brejo do Espinho (Brazil). *Hydrobiologia* **485**, 35–49. doi: 10.1023/A:1021323425591

Varejao FG, Warren LV, Simoes MG, Cerri RI, Alessandretti L, Santos MGM and Assine ML (2022) Evaluation of distinct soft-sediment deformation triggers in mixed carbonate-siliciclastic systems: Lessons from the Brazilian Pre-Salt analogue Crato Formation (Araripe Basin, NE Brazil). *Marine & Petroleum Geology* **140**, 105673.

Vasconcelos C and McKenzie JA (1997) Microbial mediation of modern dolomite precipitation and diagenesis under anoxic conditions (Lagoa Vermelha, Rio de Janeiro, Brazil). *Journal of Sedimentary Research* **67**, 378–390. doi: 10.1306/D4268577-2B26-11D7-8648000102C1865D

Vollemer T, Ricken W, Weber M, Tougiannidis N, Rohling H-G and Hambach U (2008) Orbital control on Upper Triassic Playa cycles of the Steinmergel-Keuper (Norian): A new concept for ancient playa cycles. *Palaeogeography, Palaeoclimatology, Palaeoecology* **267**, 1–16.

Warrington G (1974) Studies in the palynological biostratigraphy of the British Trias. I. Reference sections in West Lancashire and North Somerset. *Revue Palaebotanique Palynologie* **17**, 133–147.

Warrington G, Audley-Charles MG, Elliott RE, Evans WB, Ivimey-Cook HC, Kent PE, Robinson PL, Shotton FW and Taylor FM (1980) The Triassic - correlation of Triassic rocks in the British Isles. *Geological Society of London Special Report* **13**.

Waters RA and Lawrence DJD (1987) *The Geology of the South Wales Coalfield. Part III. The Country around Cardiff.* 3rd edition. Memoir of the British Geological Survey, Sheet 263.

Wright VP (2022) The mantle, CO_2 and the giant Aptian chemogenic lacustrine carbonate factory of the South Atlantic: Some carbonates are made, not born. *Sedimentology* **69**, 47–73.

Wright VP and Barnett AJ (2015) An abiotic model for the development of textures in some South Atlantic early Cretaceous lacustrine carbonates. *Geological Society of London Special Publication* **418**, 209–219.

Wright VP and Barnett AJ (2017) Critically evaluating the current depositional models for the Pre-salt Barra Velha Formation, Offshore Brazil. *AAPG Search and Discovery Article* **#51439**.

Wright VP and Sandler A (1994) A hydrogeological model for the early diagenesis of late Triassic alluvial sediments. *Journal of the Geological Society of London* **151**, 897–900.

Yang RC, Jin ZJ, Van Loon AJ, Han ZZ and Fan AP (2017) Climatic and tectonic controls of lacustrine hyperpycnite origination in the Late Triassic Ordos Basin, central China: implications for unconventional petroleum development. *AAPG Bulletin* **101**, 95–117.

Yu K, Du S, Cao Y, Zhang T (2024) Opaline silica precipitations in the Permian Fengcheng Formation indicate hot spring environments in north Mahu Sag, NW China. *Marine & Petroleum Geology* **166**, 106924.

Zavala C, *et al.* (2020) Lacustrine sequence stratigraphy: New insights from the study of the Yanchang Formation (Middle-Late Triassic), Ordos Basin, China. In *The Ordos Basin.* Elsevier. doi: 10.1016/B978-0-323-85264-7.00012-6.

Zhang F, Xu H, Konishi H, Kemp JM, Roden EE and Shen Z (2012) Dissolved sulfide-catalyzed precipitation of disordered dolomite: Implications for the formation mechanism of sedimentary dolomite. *Geochimica Cosmochimica Acta* **97**, 148–165. doi: 10.1016/j.gca.2012.09.008

Zhang F, Xu H, Shelobolina ES, Konishi H, Converse B, Shen Z and Roden ER (2015) The catalytic effect of bound extracellular polymeric substances excreted by anaerobic microorganisms on Ca-Mg carbonate precipitation: Implications for the "dolomite problem". *American Mineralogist* **100**, 483–494.

Zhao Y, Wei X, Han Z, Han C, Gao X, Meng R, Wang Q, Tucker ME, Minghui L and Sánchez-Román M (2023) Lacustrine-evaporitic microbial dolomite from a Plio-Pleistocene succession recovered by the SG-1 borehole in the Qaidam Basin, NE Tibetan Plateau. *Chemical Geology* **622**, 121376. doi: 10.1016/j.chemgeo.2023.121376